ELECTROSTATIC SURFACE STRUCTURES OF COAL AND MINERAL PARTICLES

Identification Number: DE-FG22-96PC96202-04

Grant Period: October 1, 1996 to September 30, 1999

Semiannual Technical Progress Report

April 1, 1998 to September 30, 1998

Submitted by

M.K. Mazumder (PI), D. Lindquist (Co-PI), and K.B. Tennal (Co-PI)
University of Arkansas at Little Rock
2801 S. University
Little Rock, AR 72204

Submitted to

Document Control Center
U.S. Department of Energy
Pittsburgh Energy Technology Center
PO Box 10940, MS 921-118
Pittsburgh, PA 15236-0940

December 1998

ELECTROSTATIC SURFACE STRUCTURES OF COAL AND MINERAL PARTICLES
Identification Number: DE-FG22-96PC96202
Principal Investigator: Malay K. Mazumder
Semiannual Technical Report: April 1-September 30, 1998

ABSTRACT

It is the purpose of this research to study electrostatic charging mechanisms related to electrostatic beneficiation of coal with the goal of improving models of separation and the design of electrostatic separators. Areas addressed in this technical progress report are (a) electrostatic beneficiation of Pittsburgh #8 coal powders as a function of grind size and processing atmosphere; (b) the use of fluorescent micro-spheres to probe the charge distribution on the surfaces of coal particles; (c) the use of electrostatic beneficiation to recover unburned carbon from flyash; (d) the development of research instruments for investigation of charging properties of coal.

Pittsburgh #8 powders were beneficiated as a function of grind size and under three atmosphere conditions: fresh ground in air , after 24 hours of air exposure, or under N_2 atmosphere. The feed and processed powders were analyzed by a variety of methods including moisture, ash, total sulfur, and pyritic sulfur content. Mass distribution and cumulative charge of the processed powders were also measured. Fresh ground coal performed the best in electrostatic beneficiation. Results are compared with those of similar studies conducted on Pittsburgh #8 powders last year (April 1, 1997 to September 30, 1997).

Polystyrene latex spheres were charged and deposited onto coal particles that had been passed through the electrostatic separator and collected onto insulating filters. The observations suggest bipolar charging of individual particles and patches of charge on the particles which may be associated with particular maceral types or with mineral inclusions.

A preliminary investigation was performed on eletrostatic separation of unburned carbon particles from flyash. Approximately 25% of the flyash acquired positive charge in the copper tribocharger. This compares with 75% of fresh ground coal. The negatively charged material had a slightly reduced ash content suggesting some enrichment of carbonaceous material. There was also evidence that the carbon is present at a higher ratio in larger particles than in small particles.

An ultraviolet photoelectron counter for use in ambient atmosphere is nearing completion. The counter will be used to measure work functions of different maceral and mineral types in the coal matrix. A Particle Image Analyzer for measuring size and charge of airborne particles is also under contruction and its current status is presented. A charged, monodisperse, droplet generator is also being constructed for calibration of the Particle Image Analyzer and other airborne particle analyzers in our labs.

ELECTROSTATIC SURFACE STRUCTURES OF COAL AND MINERAL PARTICLES
Identification Number: DE-FG22-96PC96202
Principal Investigator: Malay K. Mazumder
Semiannual Technical Report: April 1-September 30, 1998

TABLE OF CONTENTS

ELECTROSTATIC SURFACE STRUCTURES OF COAL AND MINERAL PARTICLES

Identification Number: DE-FG22-96PC96202
Semiannual Report: April 1-September 30, 1998

Principal Investigator: Malay K. Mazumder
Co-Principal Investigators: Kevin B. Tennal and David Lindquist
Visiting Faculty: Kathy Farley
Students: Adam Brown, Steve O'Connor, and John Jacob
University of Arkansas at Little Rock
2801 S. University
Little Rock, AR 72204-1099
Telephone: (501) 569-8007 Fax: (501) 569-8020
E-mail: mazumder@eivax.ualr.edu

Submitted to: Document Control Center
U.S. Department of Energy
Federal Energy Technology Center
PO BOX 10940, MS 921-118
Pittsburgh, PA 15236-0940

EXECUTIVE SUMMARY

The purpose of this project is to advance the fundamental understanding of the electrostatic charging properties of coal and mineral particles with the goal of improving models of electrostatic beneficiation and the design of electrostatic separators. The research involves analyzing the chemical, physical and electronic state characteristics of coal surfaces and distinguishing these characteristics between different maceral types. Areas addressed in this technical progress report are (a) electrostatic beneficiation of Pittsburgh #8 coal powders as a function of grind size and processing atmosphere; (b) the use of fluorescent micro-spheres to probe the charge distribution on the surfaces of coal particles; (c) the use of electrostatic beneficiation to recover unburned carbon from flyash; and (d) the development of research instruments for investigation of charging properties of coal.

I. INTRODUCTION

In this technical progress report, work performed in the following areas is discussed:

a. Electrostatic beneficiation of Pittsburgh #8 coal powders was examined as a function of grind size and as a function of the processing atmosphere. The feed and processed powders were analyzed by a variety of methods including moisture, ash, total sulfur, and pyritic sulfur content. Also, the mass balance and cumulative charge of the processed powders were measured. Fresh ground Pittsburgh #8 coal was found to perform the best in electrostatic beneficiation relative to

coal 24 hours after grinding and to processing in a nitrogen atmosphere. Results are compared with those of similar studies conducted on Pittsburgh #8 powders last year (April 1, 1997 to September 30, 1997).

b. The use of fluorescent micro-spheres to probe the charge distribution on the surfaces of coal particles was investigated. Experiments were performed in which 0.54μm diameter polystyrene latex spheres were charged and deposited onto coal particles that had been passed through the electrostatic separator and collected onto insulating filters. The observations suggest bipolar charging of individual particles and hot spots of charge which may be associated with particular maceral types or with mineral inclusions.

c. A preliminary investigation was performed on electrostatic separation of unburned carbon particles from flyash. Approximately 25% of the flyash was charged positively in the copper tribocharger. This compares with 75% of fresh ground coal. The negatively charged material had a slightly reduced ash content suggesting some enrichment of carbonaceous material. There was also evidence that the carbon is present at a higher ratio in larger particles than in small particles.

d. Progress is reported on the development of instrumentation related to surface and charge measurement. The UV photoelectron counter for use in ambient atmosphere is nearing completion. The status of the second prototype the Particle Image Analyzer for measuring size and charge of airborne particles is described. A charged, monodisperse, droplet generator is also being constructed for calibration of the Particle Image Analyzer and other airborne particle analyzers in our labs.

II. WORK PERFOMED

A. ELECTROSTATIC BENEFICIATION of PITTSBURGH #8 POWDERS

A major portion of this report concerns analyses of Pittsburgh #8 coal. The experimental work was performed by Ms. Kathy Farley, an Arkansas high school chemistry teacher. Ms. Farley worked this past summer under the auspices of the NSF STRIVE program directed by Dr. Jim Winters and Dr. Janet Lanza at UALR. We are indebted to her for many and varied analyses conducted on feed and processed coal powders. Specifically, moisture, ash, total sulfur, pyritic sulfur, beneficiation mass balance, and cumulative charge determinations are delineated below. The results of the beneficiation studies conducted during the past 6 months were compared to similar studies reported a year ago under this grant.

Sample Preparation:

Size classification of the powders was used as a variable in electrostatic beneficiation. Also, the effects of using an inert N_2 atmosphere and alternatively, exposing coal powders to air for 24 hours prior to processing were investigated. The three types of samples are designated **fresh ground**, **24 hr**, and **N_2**. To prepare classified coal powder, briquet sized coal pieces (from the same stock of Pittsburgh #8 coal used in studies reported a year ago) were ground coarsely with a hand grinder followed by fine grinding with a small electric grinder. The ground coal was

mechanically shaken for a minimum of 20 minutes through a stack of progressively finer sieves (150, 105, 75, 45 μm). Typically, only a third of the quantity of sub 45 micron powder went through the bottom sieve in the second 10 minutes as accumulated during the first 10 minutes of sieving. After 20 minutes each fraction was assumed to be largely depleted of sub sized powder. Sufficient quantities of 76-105 μm, 106-150 μm, 150-300 μm coal for processing and analyses were obtained; additional grinding and sieving time was necessary to accumulate enough 45-75 μm coal powder. The **fresh ground** powders were processed in succession on the same day or the following morning after storing in sealed containers. **24 hr** samples were run on different days after storing fresh ground coal in screw cap plastic containers sealed in N_2 atmosphere; each container was opened to the air 24 hours prior to beneficiation. **N_2** samples were ground in N_2 purged glove bags and processing was performed under N_2 purge with a glove bag mounted on the top of the separator.

Analysis Results:

The first collection of Figures 1 - 6 below illustrate the weight percentages of coal powder deposited on the plates of the separator as a function the total mass of feed coal used. The samples are divided according to powder collected on both the top and bottom halves of both plates of the separator. There is a deficiency in the data; where two plots share a common point only one value was measured instead of two. The abscissa of each figure is semi arbitrary; for example in Figure 1 a single value on the x-axis (45) represents a particle size range (45-75 μm). The extra points for the 106-150 μm sample of Figure 1 illustrate the measurements from two additional experiments for this sized fraction.

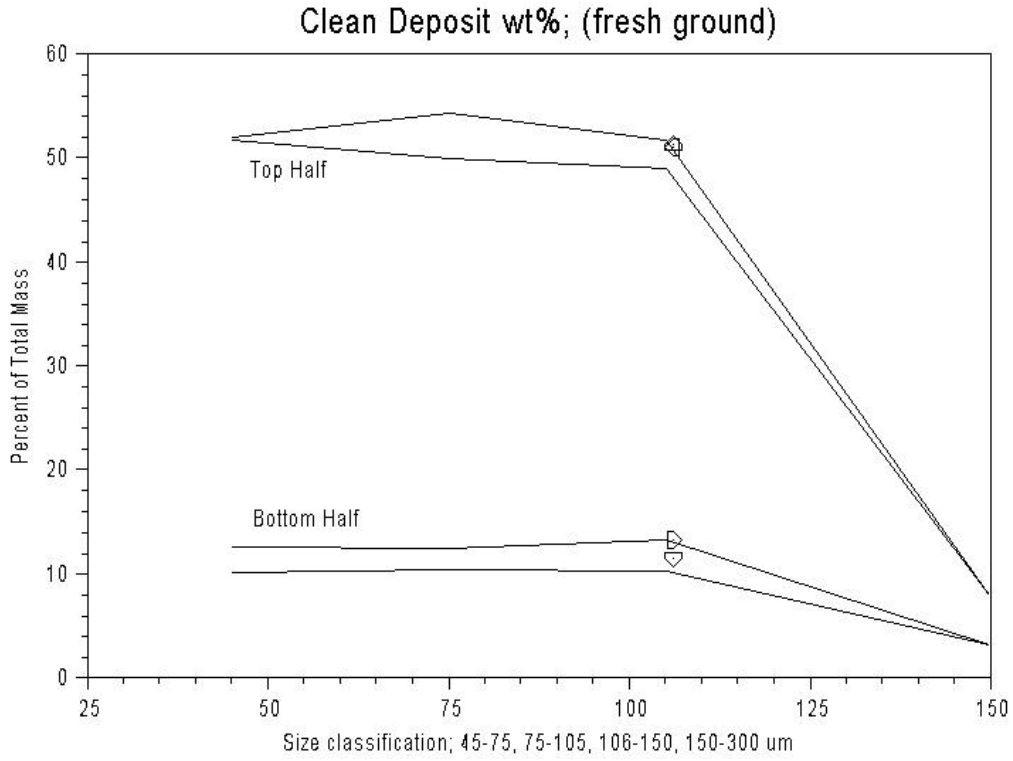

Figure 1. Percentage of fresh ground, clean coal on the separator plate.

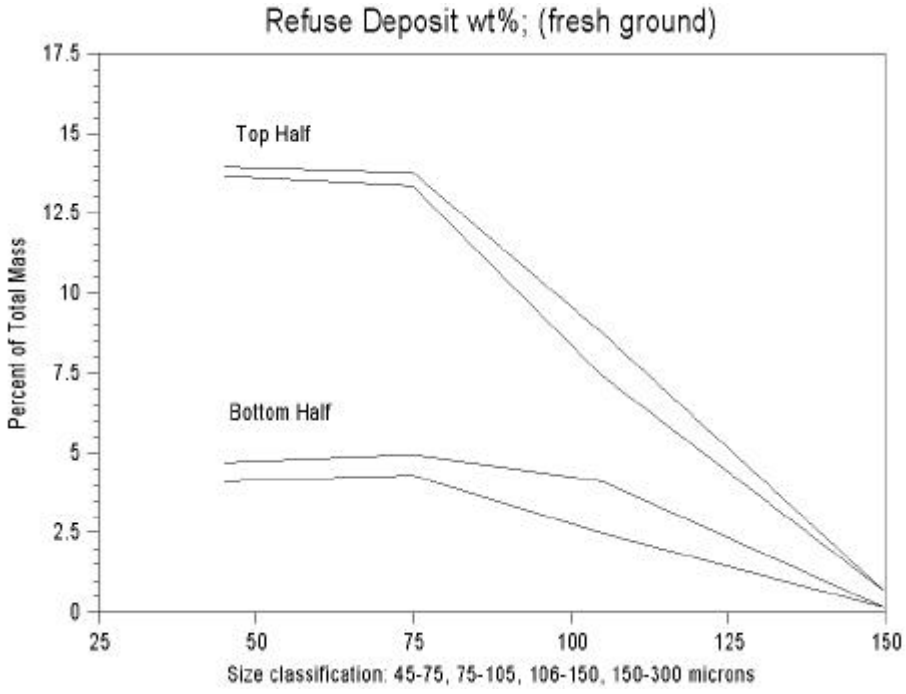

Figure 2. Percentage of fresh ground, refuses coal on the separator plate.

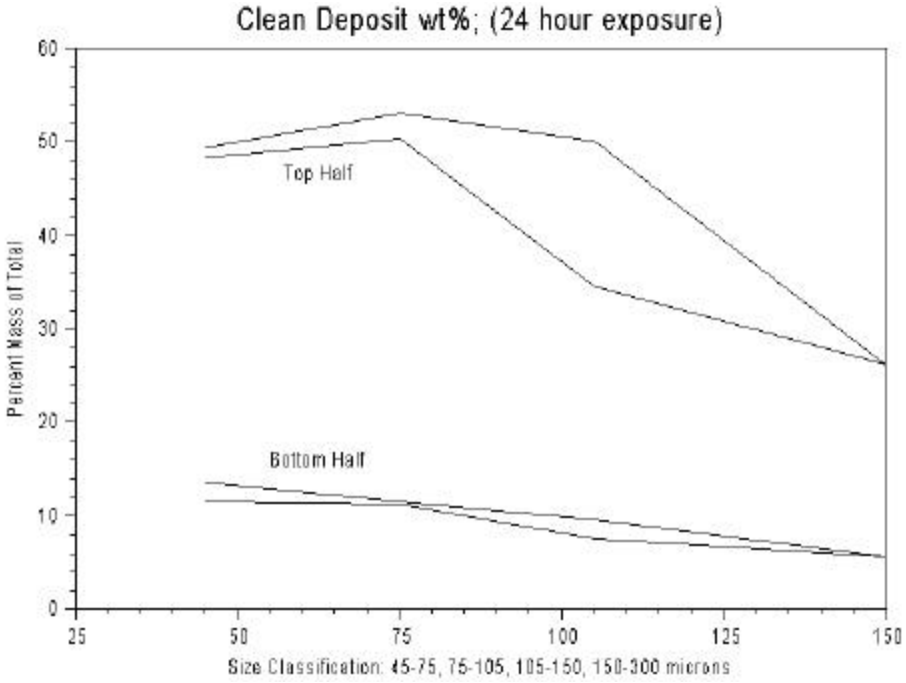

Figure 3. Percentage of 24 hr air, clean coal on the separator plate.

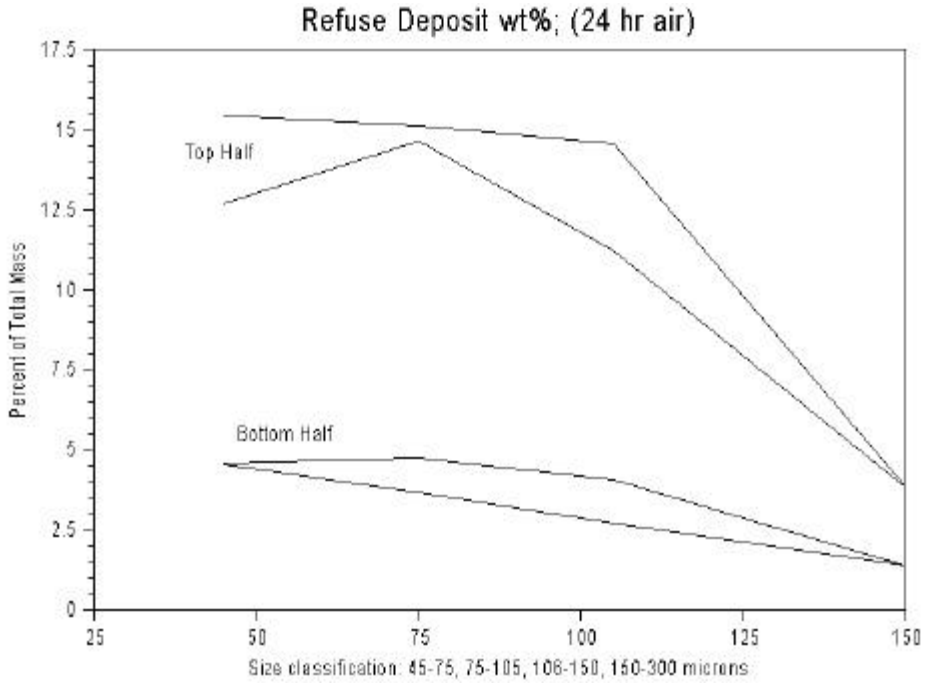

Figure 4. Percentage of 24 hr air, refuse coal on separator plate.

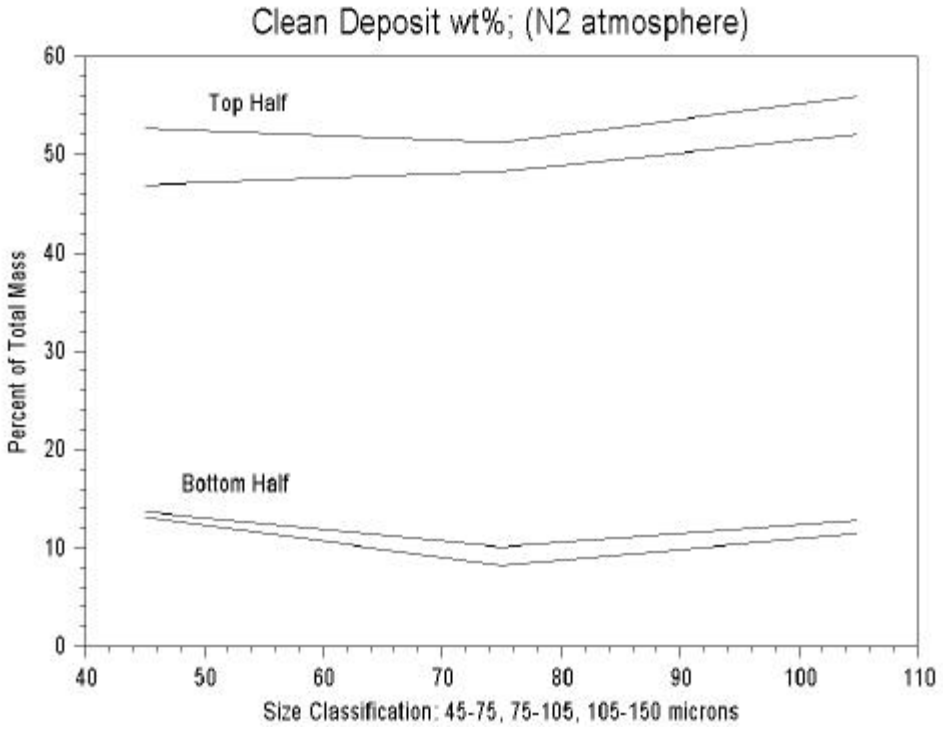

Figure 5. Percentage of N_2 clean coal on separator plate.

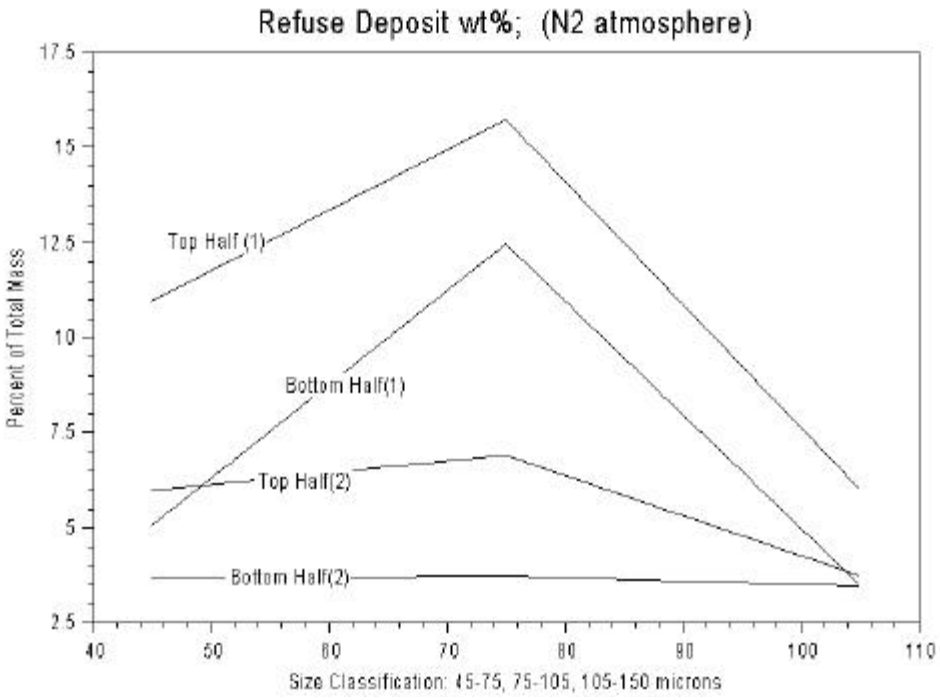

Figure 6. Percentage of N_2, refuse coal on separator plate.

In comparing Figures 1,3, and 5 there is consistency seen in the quantity of clean coal deposited on both the top and bottom halves for the three smallest size classifications whether **fresh ground**, **24 hr**, or N_2 air exposed. The extra points shown on Figure 1 corresponding to additional experimental values for 106-150 μm sized coal demonstrate the reproducibility of batches. There is a slightly greater yield of **fresh ground** clean coal among the six experiments for the smallest size classifications (45-75, 76-105, 106-150 μm). This might be accounted for by the fact that these samples were run in succession whereas the **24 hr** samples were run in batches over a period of several days. Yields were drastically reduced for the 150-300 μm **fresh ground** sample. However, only one separations experiment was conducted for this fraction. The **24 hr** 150-300 μm powder also gave a reduced yield, based on one experiment, though not as pronounced. It is seen that reduction in clean coal yields for the 150-300 μm fraction of both the **fresh ground** and **24 hr** sample were greater for the top half of the plate than for the bottom half of the clean plate deposit as would be expected for a powder containing few fines.

The weights of deposits on the refuse plate were more varied than those of the clean plate. In comparing Figures 2 and 4, it can be seen that the **24 hr** refuse weight percentage is slightly greater than that of the **fresh ground** sample particularly for the 106-150 μm sized fraction. The **24 hr** 106-150 μm sample showed a reduced total sulfur and ash content relative to the same **fresh ground** size fraction as described below. The N_2 refuse shows the most variability between batches.

Note from Figures 1,3, and 5 that only about 60% of the coal feed is retrieved as clean coal, and not all of the feed coal processed is recovered as is shown in Figures 7 and 8. Some coal passes through and is not deposited on the walls of the separator, but collects on the filter at the bottom (Figure 7). Also, since the coal is processed in batches, unaccounted weight loss of recovered coal versus feed mass are in some cases severe (Figure 8).

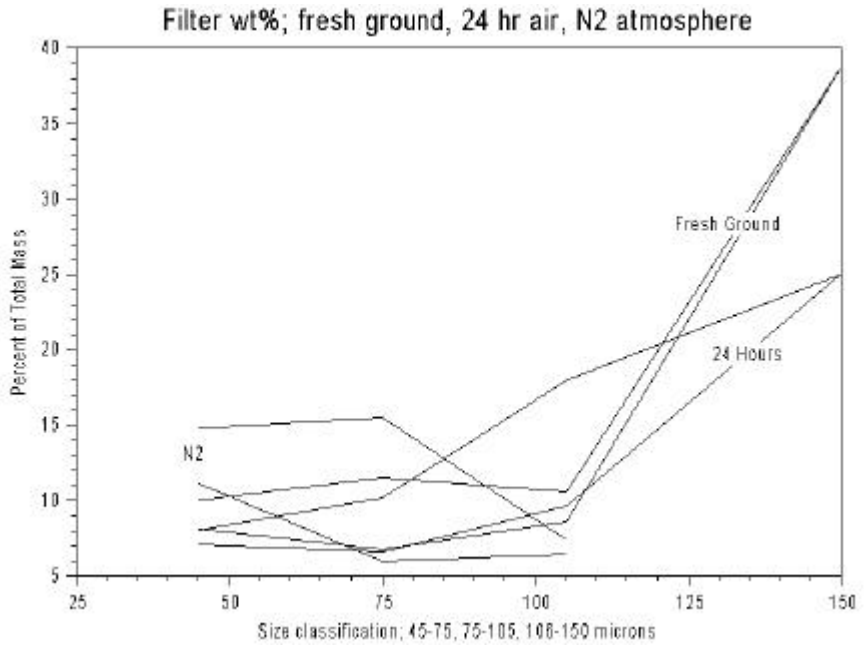

Figure 7. Weight percentage collected on filter (not deposited on separator plates).

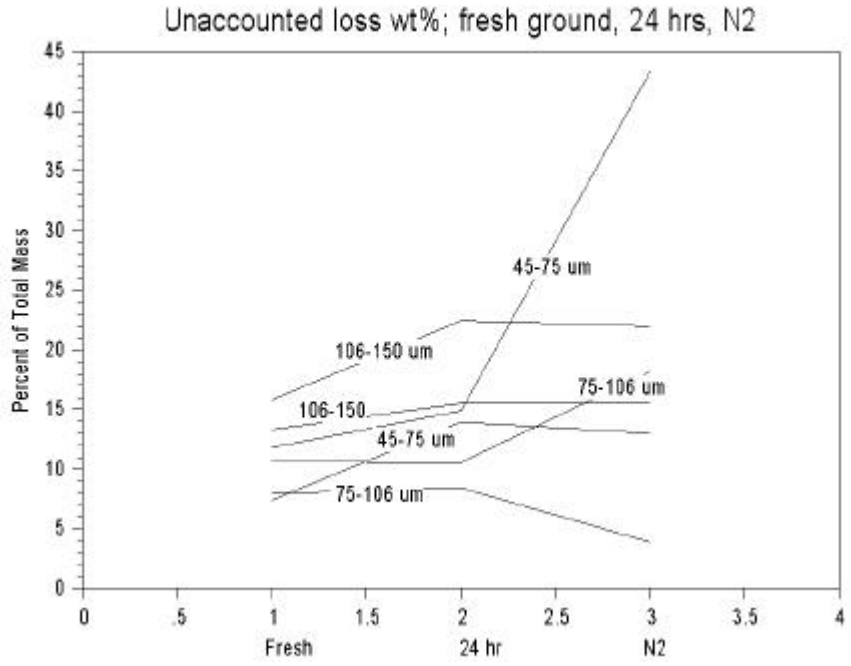

Figure 8. Unaccounted weight loss: recovered versus feed.

Some of the losses shown in Figure 8 may be attributed to material deposited inside the copper tube tribocharger and on small horizontal ledges at the bottom of the plates of the separator. It can be seen in Figure 8 that the fresh ground coal samples exhibit smaller unaccounted weight losses than the **24 hr** samples. Also, the **fresh ground** samples exhibit a narrower range of weight loss values which possibly illustrates the benefits of processing batches in succession rather than on different days.

It is firmly established that coal powders are irreversibly oxidized on exposure to air. The fact that more coal is unaccounted for in the **24 hr** sample might be attributed to coal surface oxygen coal moieties such as aldehydes, carboxylates, etc. Oxygen functions are good ligands and may enhance sticking of oxygenated powders to metal surfaces. Also, in comparing Figures 2 and 4, there is observed a greater yield on the refuse plate of the **24 hr** sample than for that of the **fresh ground** sample, consistent with expected negative charging of oxygenated coal powder.

The great variability in data from the two $\mathbf{N_2}$ separations experiments makes any conclusions drawn from data from these samples suspect. As seen in Figure 8, unaccounted for weight losses for the two smallest particle size ranges processed in $\mathbf{N_2}$ are quite high. This might be attributed to turbulent flow in the separator since N_2 purge is introduced at the top of the separator from a high pressure cylinder. These results suggest a lower charge to mass ratio for these large powders since smaller highly charged powder particles would have deposited first on exiting the tribocharger. The $\mathbf{N_2}$ 150-300 μm sample was not processed.

Figure 9 below is taken from last year's report (Figure 6 April 1997-September 1997).

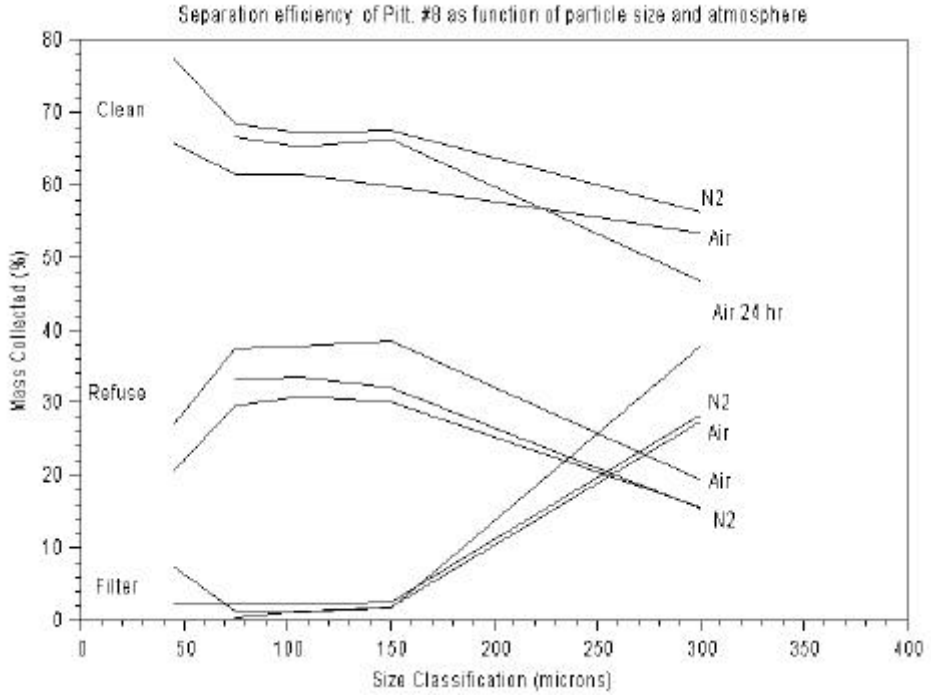

Figure 9. 1997 data on Pittsburgh #8 Coal Powders (Percentages are based on weight of recovered coal only).

The data in Figure 9 differs from that of Figures 1-7 in that mass percentages are based only upon the weight of recovered coal, rather than the weight of feed coal. Therefore, the mass percentages of Figure 9 are biased to larger values than those of Figures 1-7. The values used for Figure 9 will be recalculated to allow a fair comparison with data collected this year.

However, a quick inspection of Figure 8 illustrates that unaccounted weight losses range approximately from 5 wt% to 25 wt% in samples processed this year. By taking these weight losses into account, the weight percentages of refuse and clean deposits collected this year compare favorably to those of the previous study. Therefore, Pittsburgh #8 coal briquets stored in a capped 5 gallon plastic bucket for one year appear to beneficiate to a similar degree as the briquets a year ago.

The similarity in weight percentage data from the two years is confirmed by other analyses. Figures 10-12 below illustrate the magnitudes of the total gravimetric sulfur analyses of feed and processed Pittsburgh #8 coal powders. The deposits on each plate from the bottom and top halves were combined in order to have sufficient coal for all analyses. In Figures 10 and 11 the line graphs represent 1998 data and the scatter points represent 1997 total sulfur data. Comparison of the scatter points and line graphs of Figures 10 and 11 indicates that the 1997 data correlates quite well with 1998 data from the same Pittsburgh #8 coal stock.

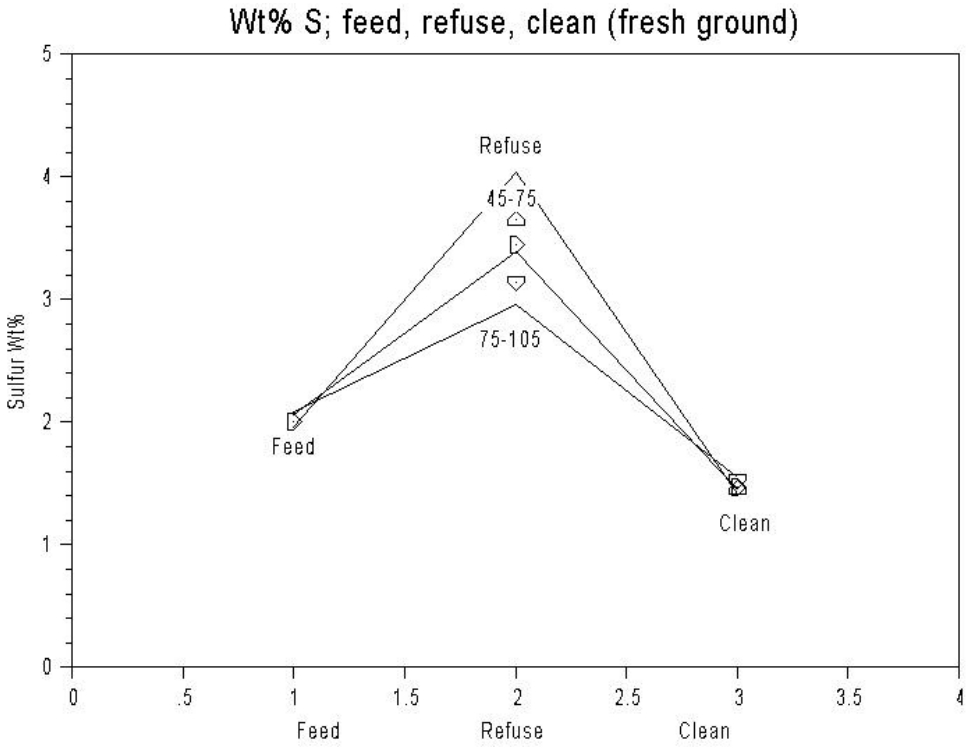

Figure 10. Total sulfur by gravimetric analysis for fresh ground sample.

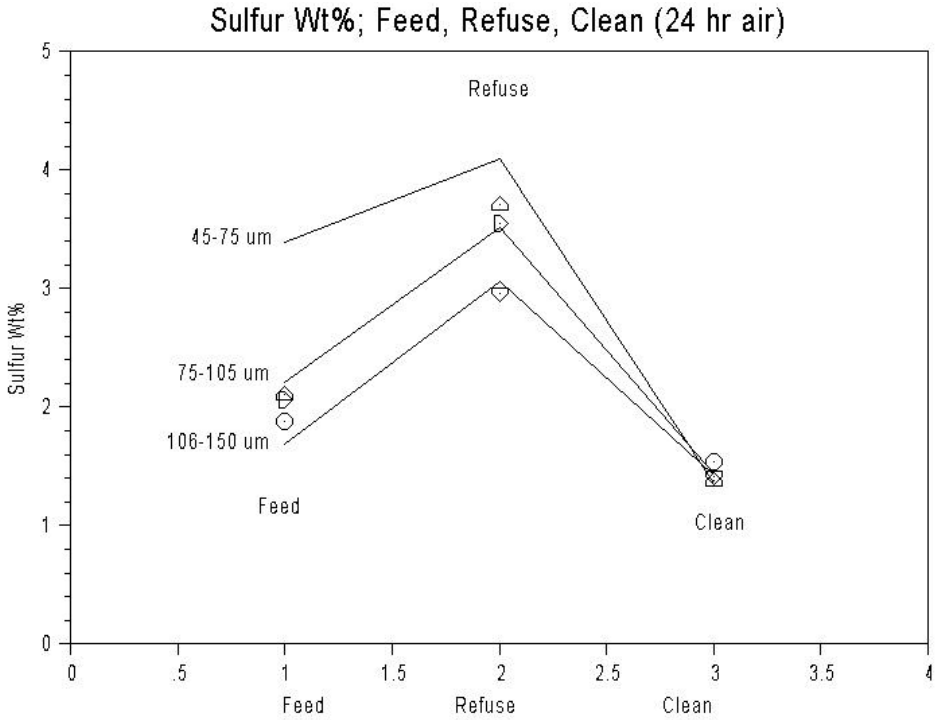

Figure 11. Total sulfur for 24 hour air sample.

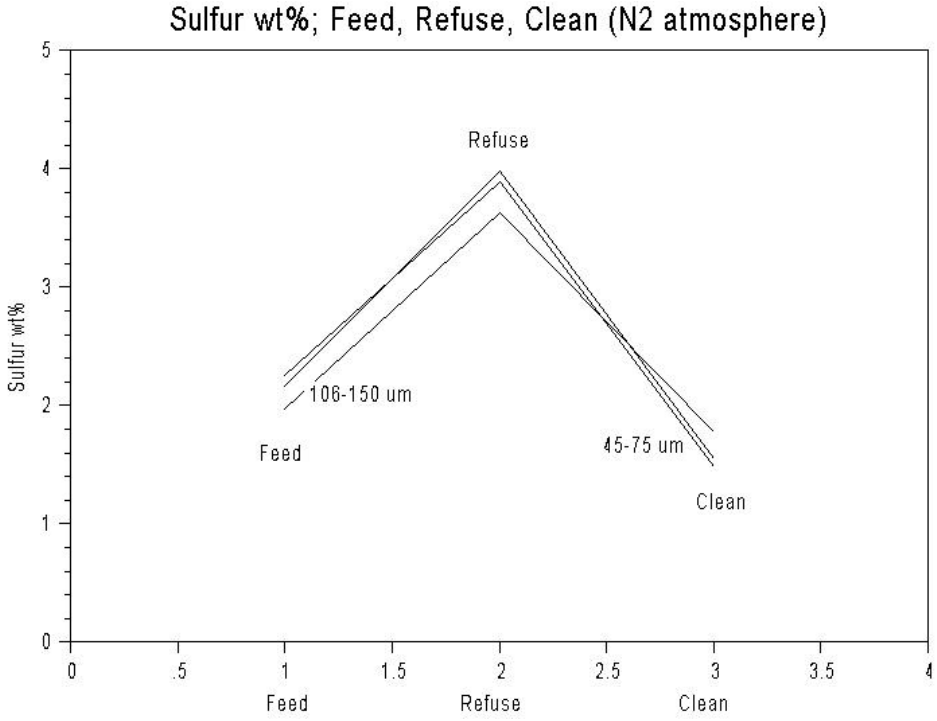

Figure 12. Total sulfur for N_2 sample.

A remarkable feature of Figures 10-12 is that the total sulfur content of the clean fractions, from experiments both this year and last, are similar regardless of the atmosphere of beneficiation or even of particle size class. This fact suggests that positively charged clean coal of a specific maceral composition is consistently deposited on the plate of the separator. Referring again to the program report of a year ago, petrographic analyses and diffuse reflectance infrared spectroscopy measurements of processed powders indicated a greater inertinite and liptinite content in the refuse fraction and a greater vitrinite content in the clean fraction relative to the feed coal. This has been attributed to associated minerals and trimacerite depositing onto the refuse plate. Therefore, the consistent total sulfur values obtained for clean coal is likely due to a composition enriched in vitrinite. The similar sulfur contents of all clean fractions indicates that a primary goal to improve beneficiation is simply to increase the weight percentage of the deposit of clean coal obtained since all of the clean powders are alike.

To date we have focused on total sulfur analyses to measure the efficacy of beneficiation; it is easier to perform total sulfur analyses in lieu of those distinguishing pyritic sulfur. However, only the pyritic sulfur fraction is theoretically amenable to electrostatic beneficiation and therefore verification is necessary. Ms. Farley obtained some values for pyritic sulfur content of feed and processed coals using ASTM Method: D 2492-84. Figure 13 shows comparative pyritic sulfur and total sulfur content data for 45-75 μm sized Pittsburgh #8 powders.

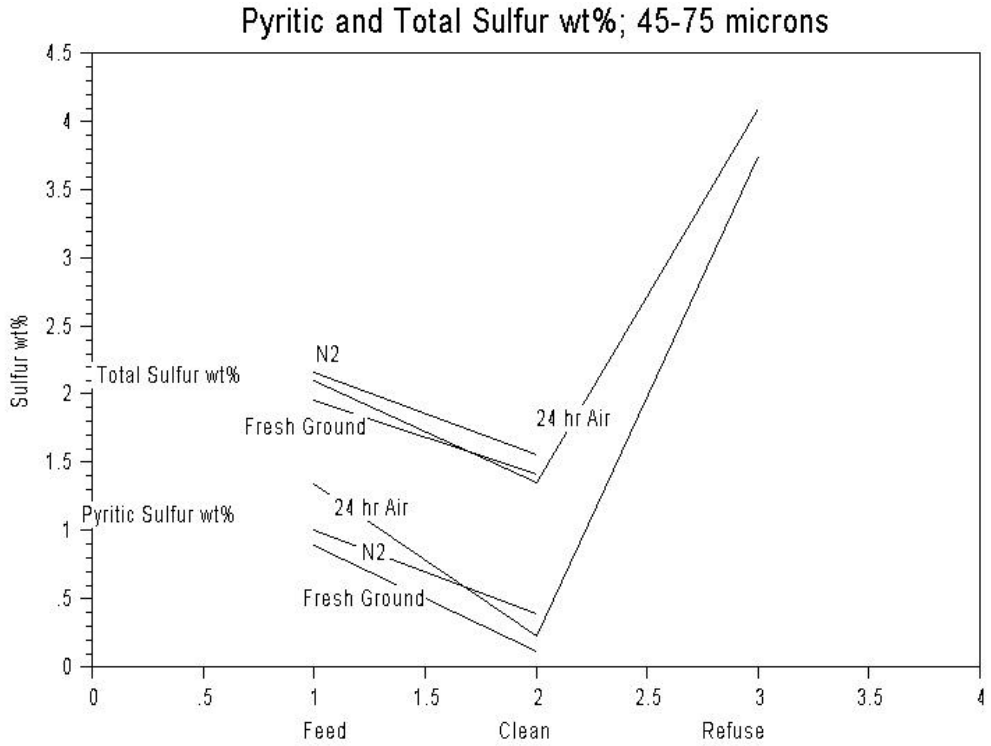

Figure 13. Comparison of total sulfur and pyritic sulfur of feed and processed 45-75 μm Pittsburgh #8 powders.

The direct relationship between pyritic sulfur and total sulfur content is readily apparent from Figure 13. Moreover, the one value obtained for the pyritic sulfur content in refuse as shown in Figure 13 does not parallel, but rather approaches the value for total sulfur. These results illustrate that indeed, pyritic sulfur is the sulfur fraction amenable to electrostatic beneficiation and concentrated in the refuse. The fact that the refuse does not contain solely pyritic sulfur is largely due to a significant quantity of macerals containing organic sulfur deposited in the refuse. Also, inspection of Figure 13 reveals that the pyritic content of these small sized powders is reduced by nearly a magnitude in clean coal relative to feed coal.

Ash analyses for feed and processed Pittsburgh #8 coal powders are illustrated in Figures 14-16.

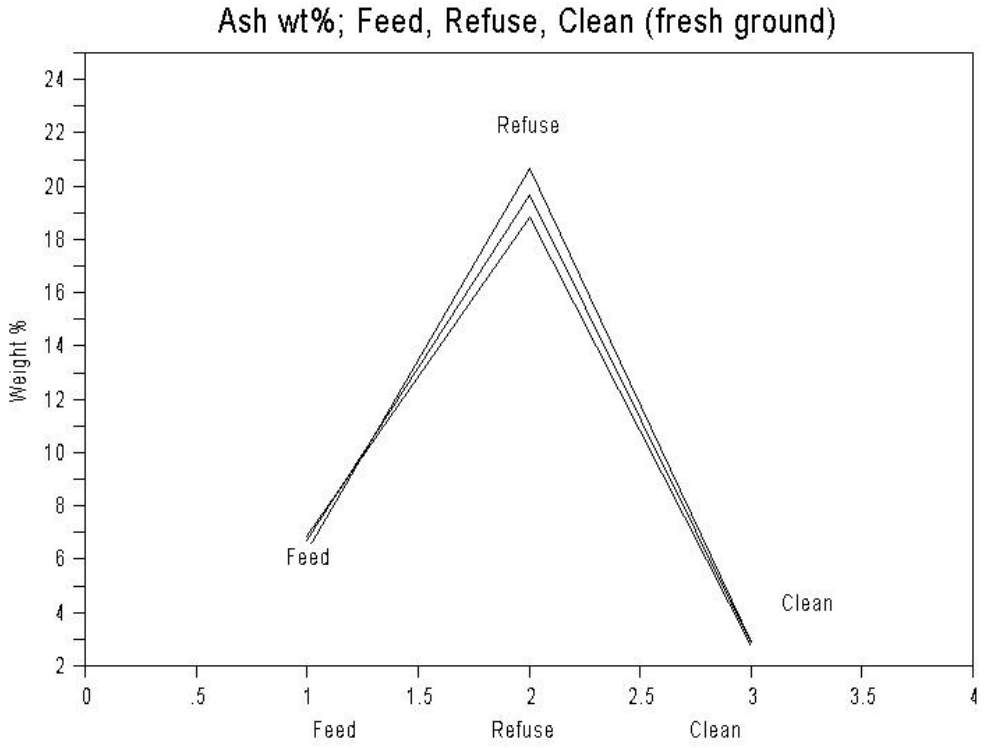

Figure 14. Weight percentage of ash in fresh ground powders.

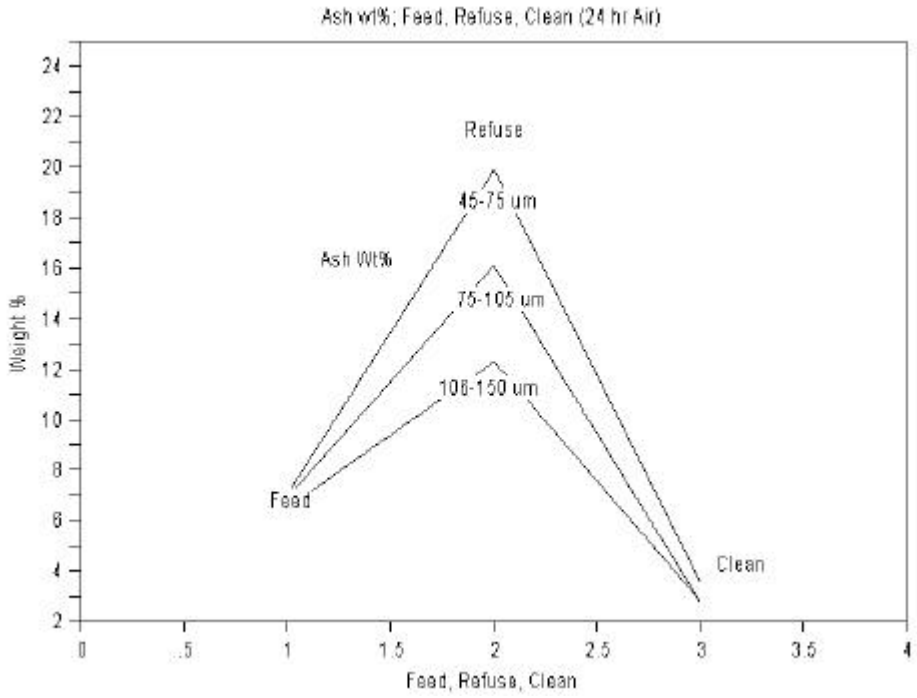

Figure 15. Weight percentage of ash in 24 hr powders.

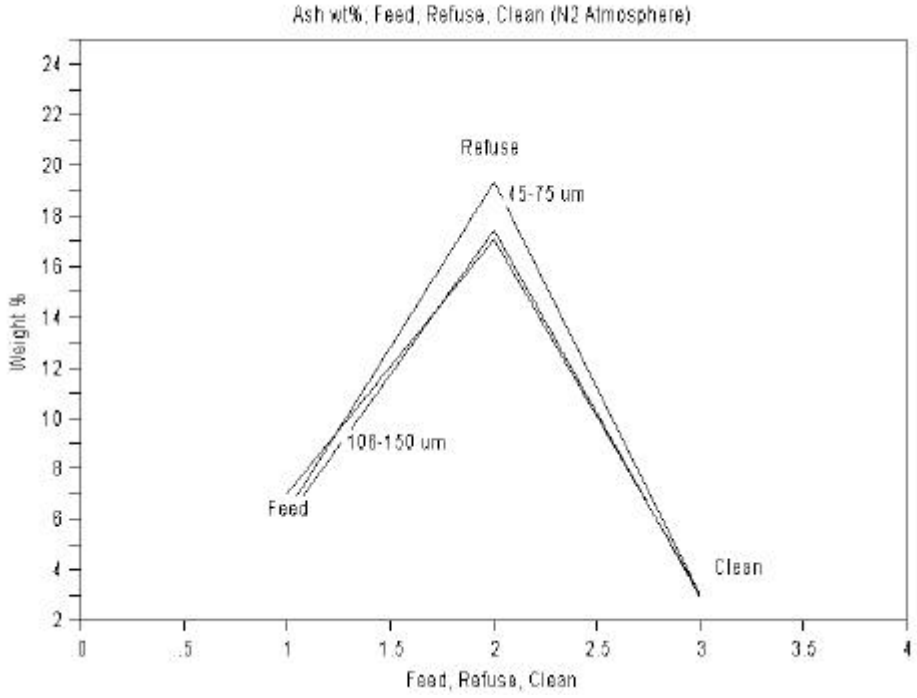

Figure 16. Weight percentage of ash in N_2 powders

In concert with the total sulfur analyses, Figures 14 through 16 illustrate that the clean coal fractions have similar ash content regardless of process atmosphere and powder size class. This is further confirmation of a specific composition in clean Pittsburgh #8 coal powders. Also, as seen for the sulfur analyses the refuse ash values are variable which is in contrast to the clean coal data. The refuse of the finest coal (45-75 μm) has the highest sulfur and ash content. This is expected due to greater liberation of pyrite and other minerals in fine powders. However, the question then arises as to why the clean coal analyses do not show similar variations? If the sulfur and ash content of the refuse increases for the smallest powders processed, the clean powder then should exhibit a decreased ash and sulfur content. Perhaps one explanation is that the unaccounted weight losses in batch electrostatic beneficiation are attributed to lost clean coal. Therefore, if the unaccounted weight loss problem is solved, the yield of clean coal will increase to a greater extent than that of the refuse fraction which is desirable.

Figures 17 through 19 show the moisture analysis values obtained according ASTM Method #D 3173-87. As expected the **24 hr** samples exhibited a higher moisture content than the **fresh ground** samples.

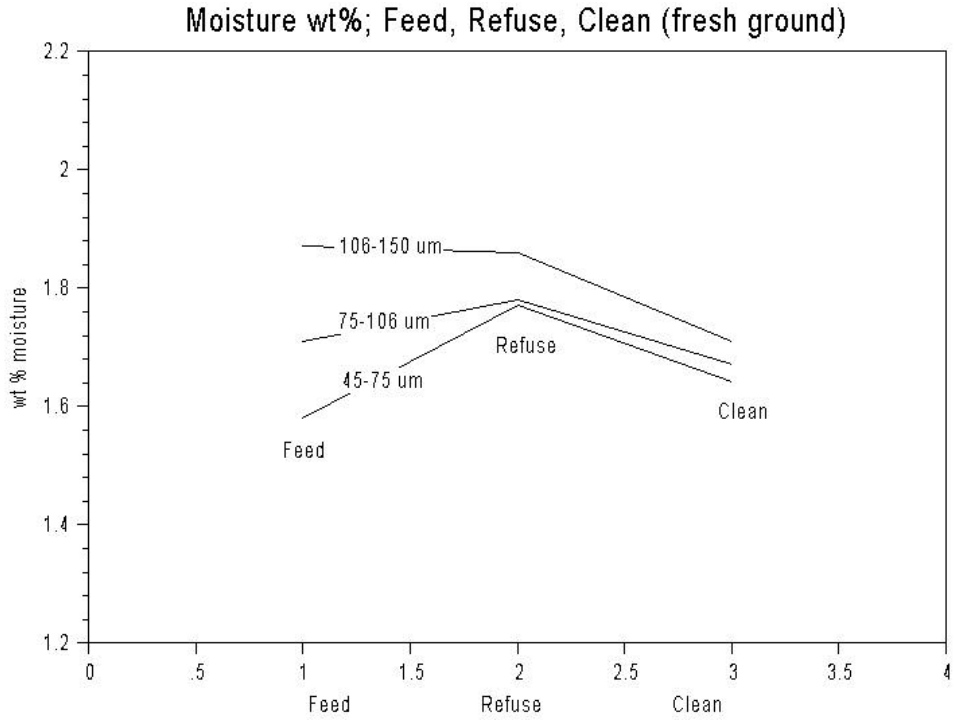

Figure 17. Moisture wt% fresh ground.

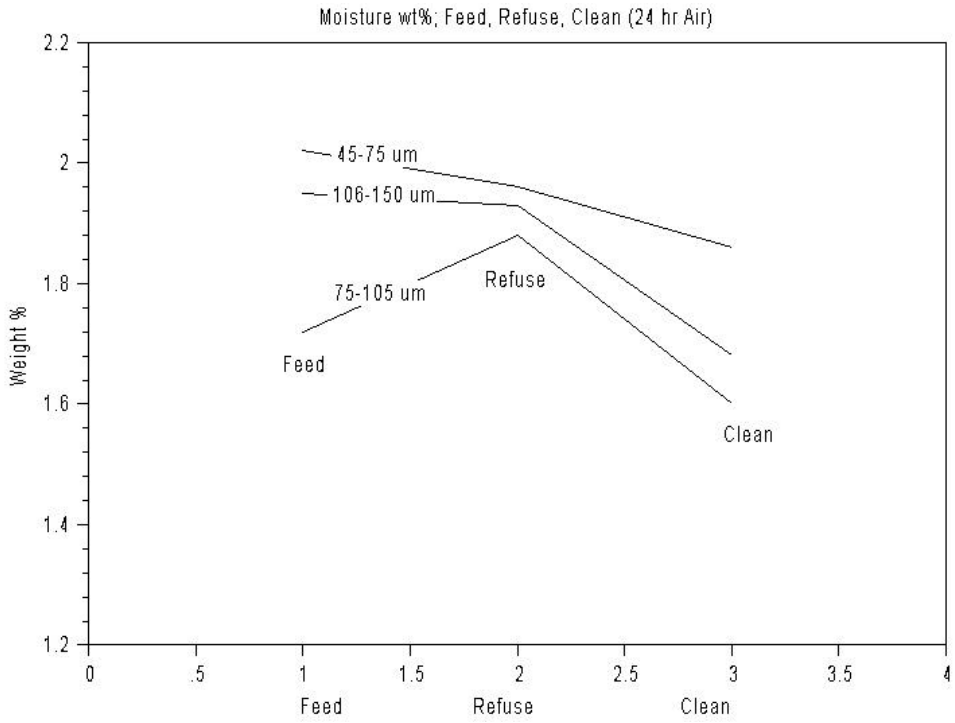

Figure 18. Moisture wt% 24 hr air.

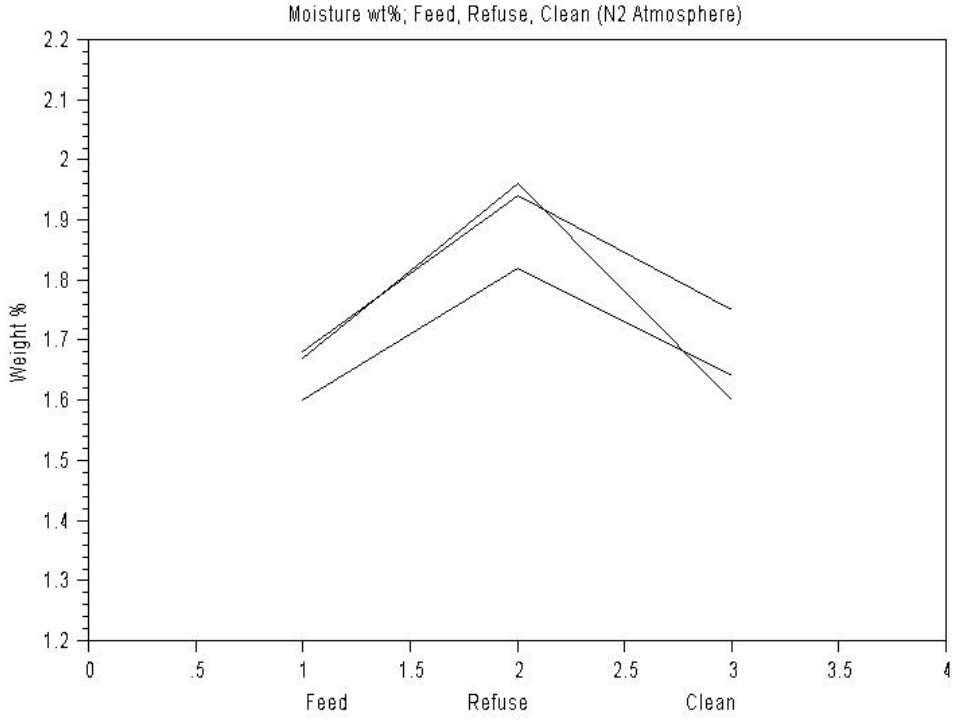

Figure 19. Moisture wt% N_2.

Finally, Figure 20 illustrates the results of the six beneficiation experiments during which the total charge and total mass of coal deposit on plates of the separator were measured for freshly ground coal processed immediately after grinding. No data was obtained for the 150-300 μm fractions of the 24 hour and N_2 treated samples. The top cluster of plots in Figure 20 represent measurements obtained from the clean (negative polarity) plate of the separator; the cluster of plots of lower charge to mass ratio represent measurements from the refuse (positive polarity) plate of the separator. Again, the most striking feature is the uniform nature of the clean coal data of Figure 20 in agreement with the other varied analyses on Pittsburgh # 8 powders.

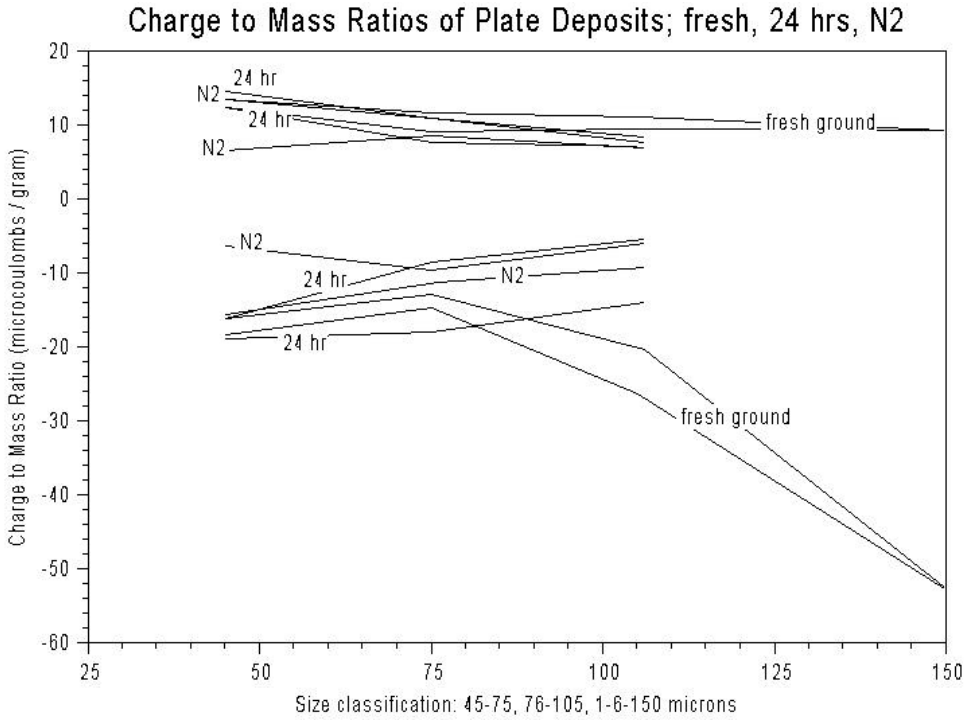

Figure 20. Charge to deposit mass ratios measured for both separator plates.

In summary one may propose a possible scenario for electrostatic beneficiation. The coal, consisting primarily of two microlithotypes: vitrite and trimacerite, is crushed to liberate the two to some extent. The consistent ash and sulfur content measured for the clean plate deposit may have a composition ascribed to the vitrite fraction since vitrite is the most uniform of the microlithotypes. Therefore, a practical limit to beneficiation may be defined by the quantity of vitrite in the coal. The extent to which vitrite is liberated and has not been surface oxidized are major factors to improve clean coal yields. Concerning the refuse, greater extraction of minerals is achieved for the finest powders. Unaccounted weight losses in batch processing may be due to clean coal powders not collected with the majority of clean coal on the negative plate of the separator, but instead lost to other surfaces of the apparatus such as inside the copper tribocharger tube.

B. CHARGE DISTRIBUTIONS USING FLUORESCENT MICRO-PARTICLES

In these experiments fluorescent micro-spheres were used to probe the charge distribution on the surfaces of coal particles. This imaging process identifies bipolar charge distributions - if present - on the particle surfaces.

Illinois #6 coal was ground and sieved. The size range 45 μm (+325 mesh) to 75μm (-200 mesh) was selected for the experiments. (Note that after sieving significant numbers of smaller particles (<45μm) remain in the distribution.) The coal particles were charged using the copper, static tribocharger. The particles passed directly from the charger into the electrostatic separator. Insulating membrane filters (and later glass slides) were attached to the electrodes of the separator.

Fluorescent, monodisperse polystyrene latex spheres (PLS) with 0.54 μm diameter were aerosolized from liquid suspension using a pneumatic jet nebulizer. They were dried as they passed through a silica gel diffusion dryer. They were then charged in a corona field created by applying a high voltage (7 to10 KV) to a hypodermic needle placed about 2.5cm from a curved grounded electrode attached to the wall on the opposite side of the respirator tubing through which the aerosol was flowing. The polarity of charge imparted to the microspheres was selected by selection of the polarity applied to the corona needle.

After collection of coal particles, one filter was removed from each of the separator plates and positioned so that the negatively charged polystyrene aerosol could flow slowly over the top of the filters. Then the remaining filters from each plate were exposed similarly to positively charged aerosol. This resulted in four situations: 1) negative PLS on positive coal, 2) negative PLS on negative coal, 3) positive PLS on negative coal and 4) positive PLS on positive coal.

The filters were examined in an epifluoresence microscope under UV illumination. Color slides were made for several areas. Several examples are included here. Figures 21 and 22 show negative PLS deposited onto positive coal. Figures 22 shows two magnified regions where one particle showed high collection while neighboring particles showed very little. In the lower part of Figure 22, taken at slightly higher magnification, the deposition was highly localized on the particle.

We did not perform detailed observations of these slides. However, several observations are noted. For negative PLS on positive coal the deposition was predominantly on the dark macerals. Occasionally, however, a liptinite maceral was found with multiple PLS particles while surrounding dark material had none. We also observed significant deposition near sharp edges of particles.

When negative PLS were used with positive coal particles nearly all of the PLS was deposited onto coal particles. When positive PLS was used with negative powder from the refuse plate, we observed a significant number of PLS that were on the filter or slide away from the coal particles. These could have been located over submicron mineral particles that were not observed in the microscope.

Figure 23 shows deposition of positively charged PLS onto positively charged coal particles. Most of the PLS landed on the filter and is not associated with coal particles. These are generally out of focus in this picture and are seen as a circular halo around a central spot. However, significant numbers of PLS did attach to the coal particles suggesting negative charge sites on coal particles with net positive charge. This same observation was made when negative

PLS was used with negative coal powder suggesting positive charge sites on the net negative particles.

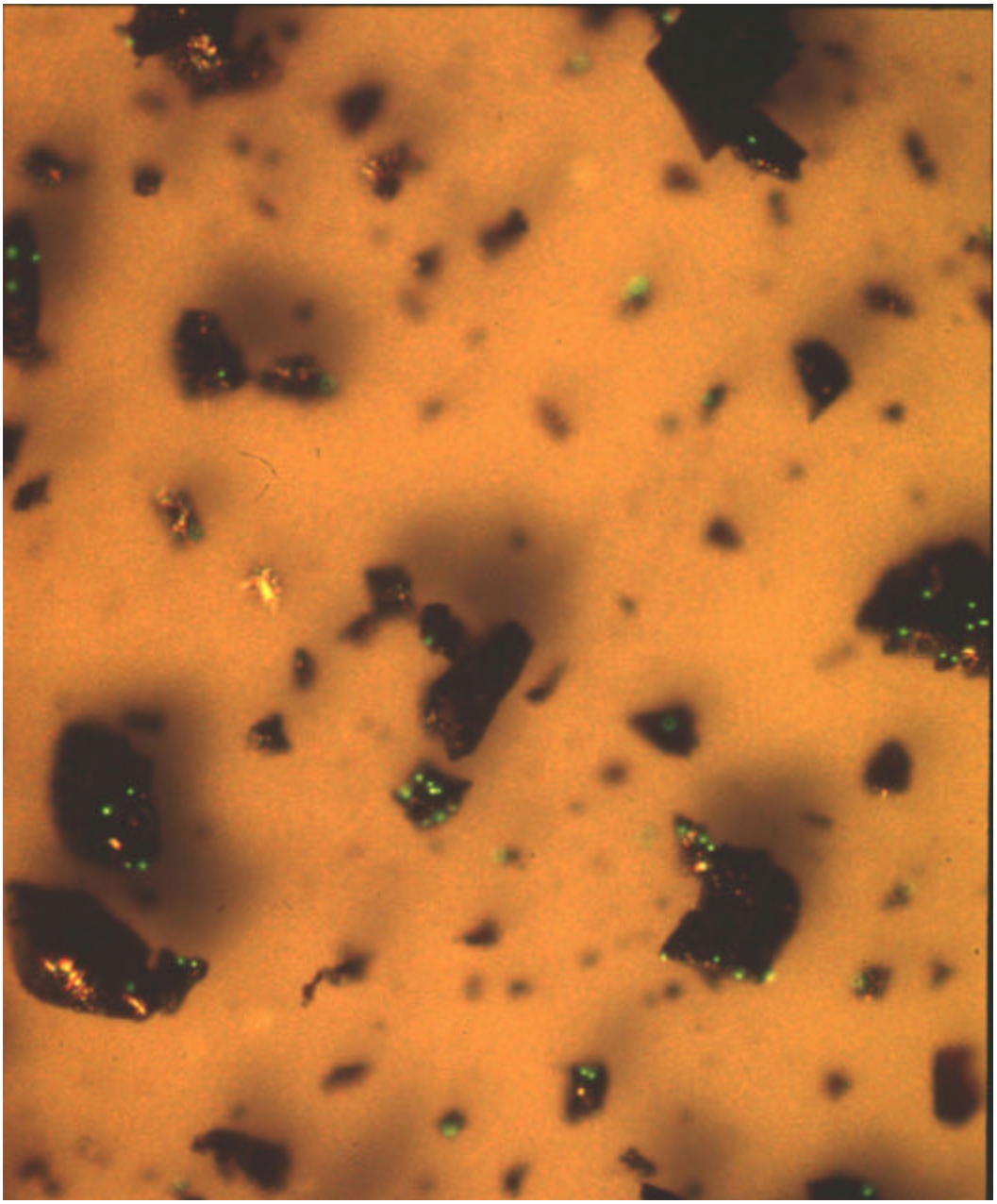

Figure 21. Deposition of negatively charged fluorescent polystyrene onto positively charged coal particles.

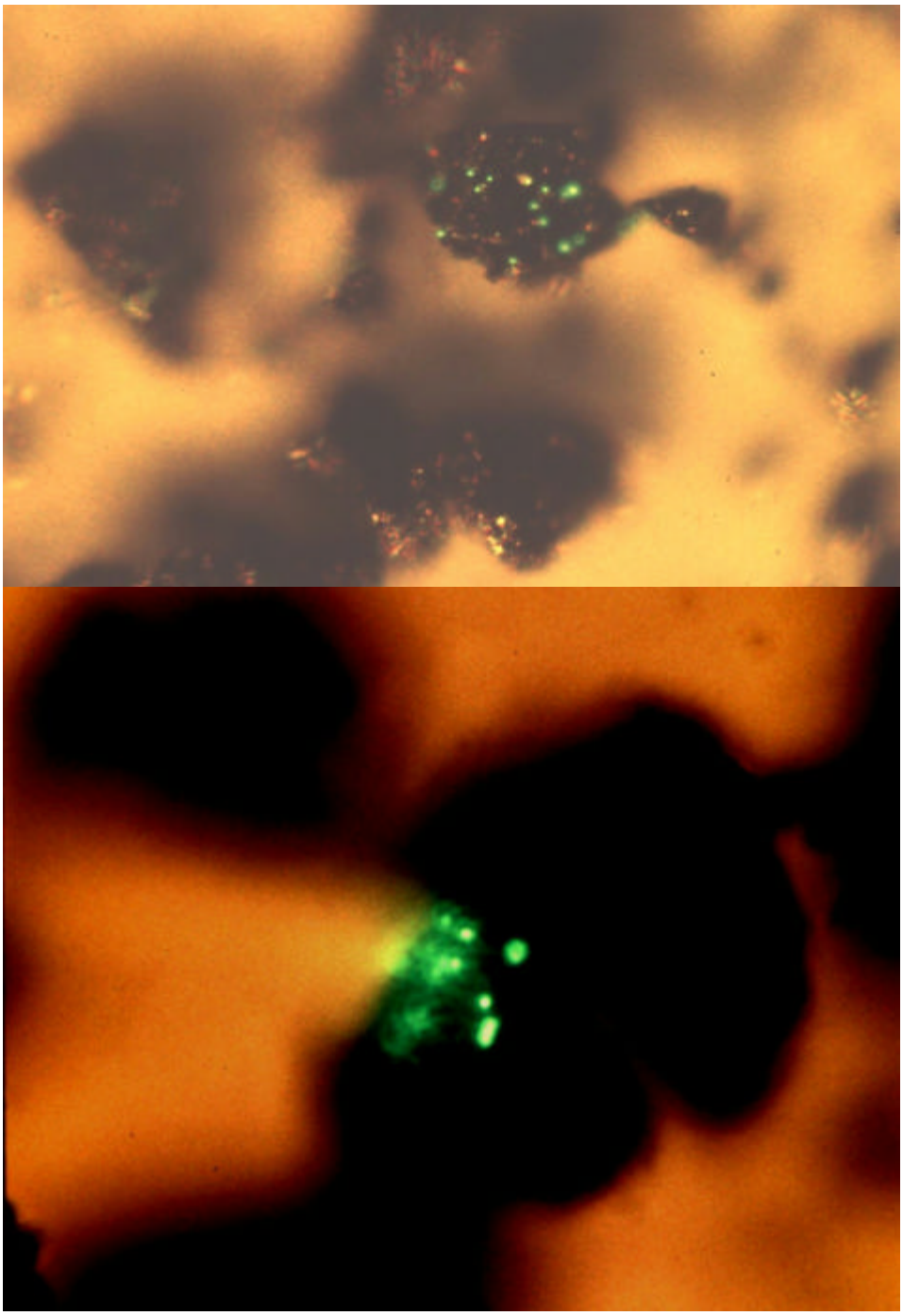

Figure 22. These two pictures show deposition of negative PLS onto positive coal. In each case one particle showed high collection while neighboring particles showed very little. In the lower picture, taken at higher magnification, the deposition was highly localized on the particle.

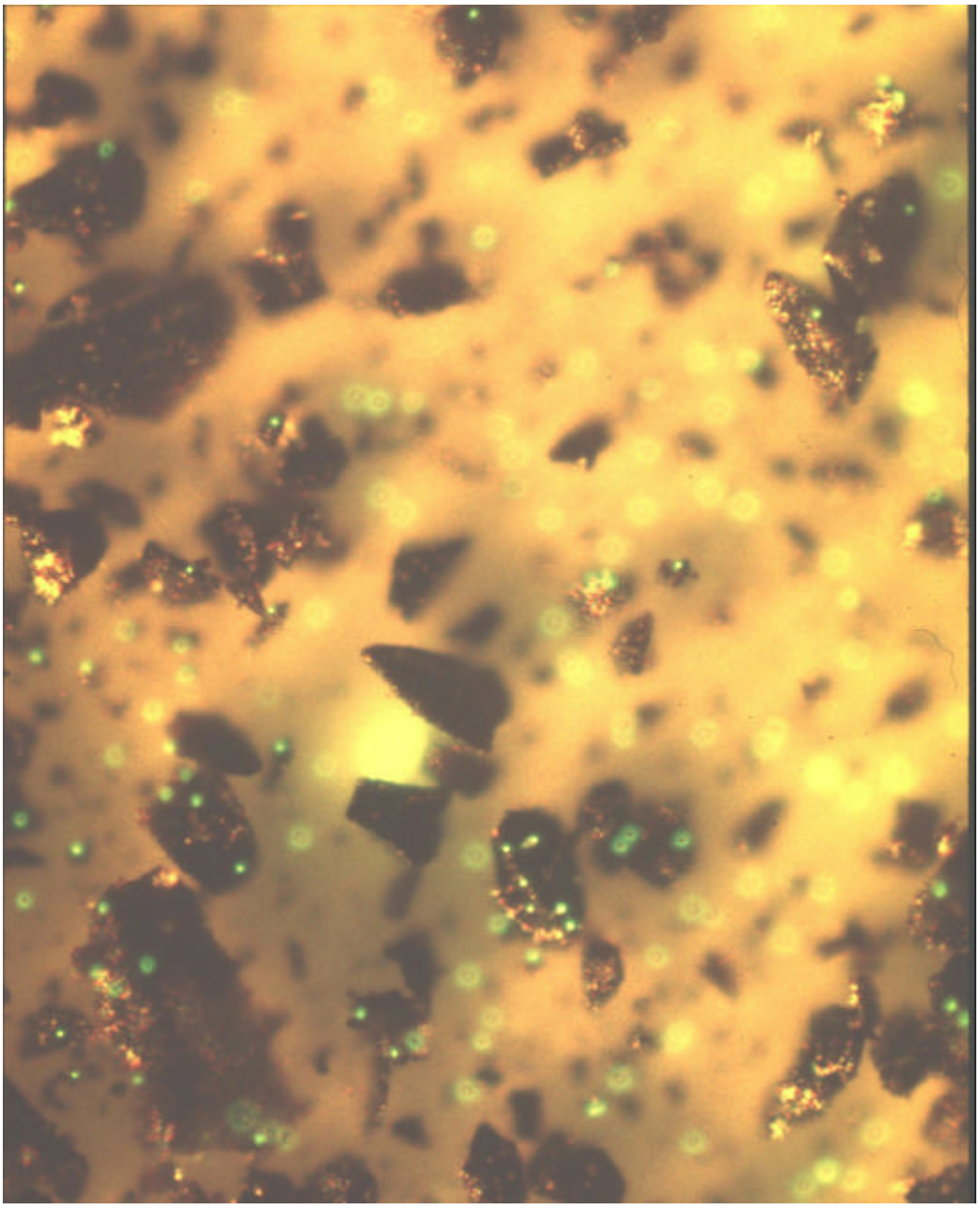

Figure 23. Deposition of positively charged fluorescent polystyrene latex spheres onto positively charged coal particles. Most of the PLS landed on the filter and is not associated with coal particles. These are generally out of focus in this picture and are seen as a circular halo around a central spot. However, significant numbers of PLS did attach to the coal particles suggesting negative charge sites on coal particles with net positive charge.

C. RECOVERY OF UNBURNED COAL FROM FLYASH

We received a sample of baghouse flyash from DOE for testing. Preliminary measurements were made to examine the feasibility of recovering unburned carbon from the flyash using electrostatic beneficiation. Measurements of the size and charge of the flyash particles were made using the particle image analyzer. Some of the sample was then passed through the copper tribocharger and the electrostatic separator. The net charge imparted to the flyash was measured and the relative masses collected on each plate were determined.

For the size and charge measurements the flyash was blown through a coiled copper tube (1/4" tube 3 turns of 3" diameter). Runs were made with flyash directly from the sample container (as received) and with flyash that was first dispersed in water and then filtered and dried.in a heated vacuum dessicator. Figure 24 shows the measured size distributions for the two cases. The measured count median diameter increased from 8.1 to 10.1 μm following the water treatment. Figure 25 shows the charge distributions for the two cases and Tables C.I and C.II show the charge summaries. For the unwashed flyash the charge distribution was slightly negative.

Two runs were made using approximately 10 grams of coal each time. Charge to mass ratio was nearly identical for the two runs at -10.75 μC/g. Note that runs with coal nearly always show a net positive charge except in cases where the coal has been oxidized. The mass fraction collected on the negative electrode was approximately 21%. While the mass fraction collected on the positive electrode was about 66%. Three percent of the powder was collected on the filter at the bottom of the separator. The remaining 10% was not recovered. Some of this was left on the vibratory feeder some on the side walls of the separator.

Standard ASTM procedures used to measure ash in coal were applied to the recovered fractions. The results are given in Table C.III. The non-ash fraction of the material collected on the positive electrode was about 10% greater than the non-ash fraction of the material collected on the negative plate for each of the two runs. This indicates that the unburned carbon material has a slightly greater probability of charging negative rather than positive. Previous experiments have shown that oxidation of coal power by exposure to air or ozone results in a shift toward negative charge.

The non-ash content of material collected on the filter was significantly higher than that of material collected on the electrodes (22% compared to around 10%). Larger particles tend to end up on the filter. Larger particles would also be more likely to be incompletely burned. This suggests that size segregation might be employed as a step in recovery of the unburned carbon from flyash. It is also possible that the carbon and mineral components of the flyash are not physically liberated from each other. This should be investigated and it should then be determined if another grinding step should be employed. The carbon does not appear to be preferentially charged to the opposite polarity to which the minerals are charged. Thus, this method of electrostatic beneficiation may not be feasible for recovering the unburned carbon. It might still be possible to use electrostatic separation based on particle resistivity. This is a different technique than currently applied in our lab.

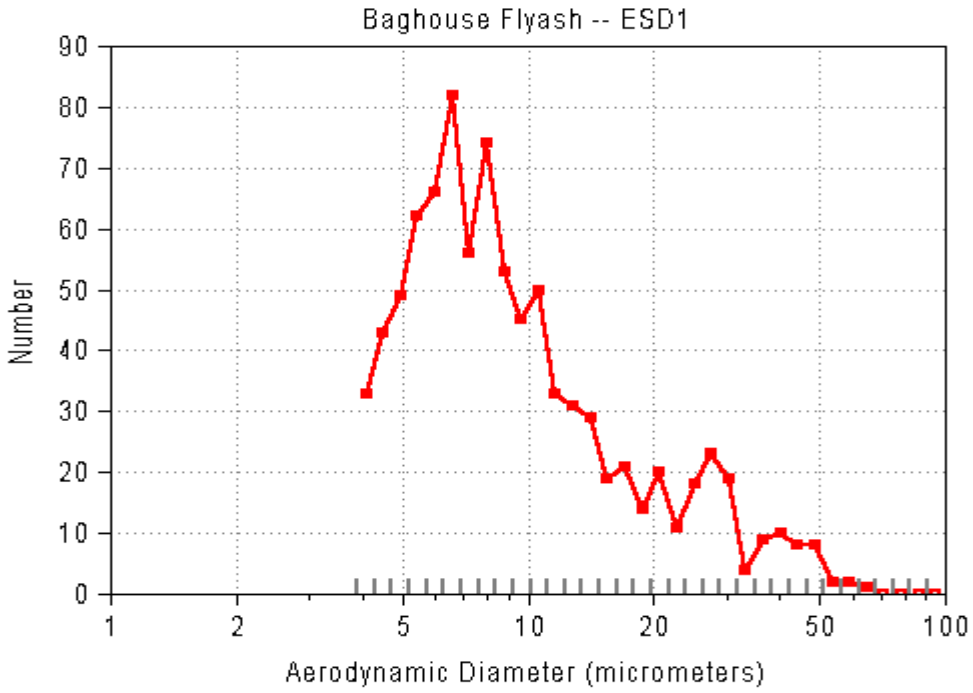

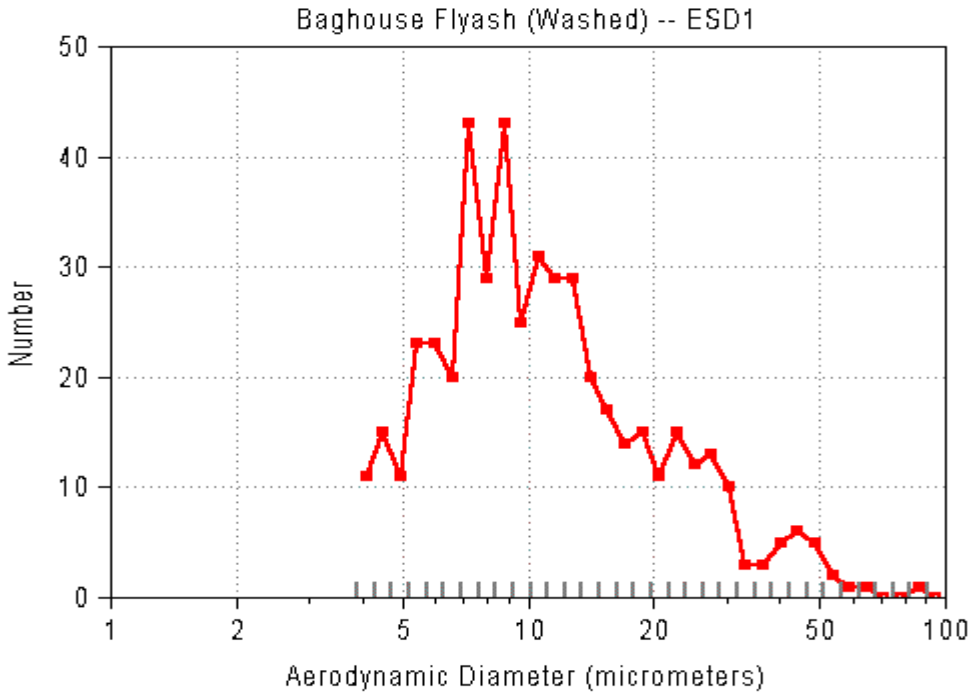

Figure 24. Size distributions for baghouse flyash measured with the particle image analyzer. In both cases the flyash was blown through a copper coiled copper tube. The top plot (A) shows the size for the virgin flyash. The bottom curve is for flyash that was first dispersed in water and then filtered and dried.

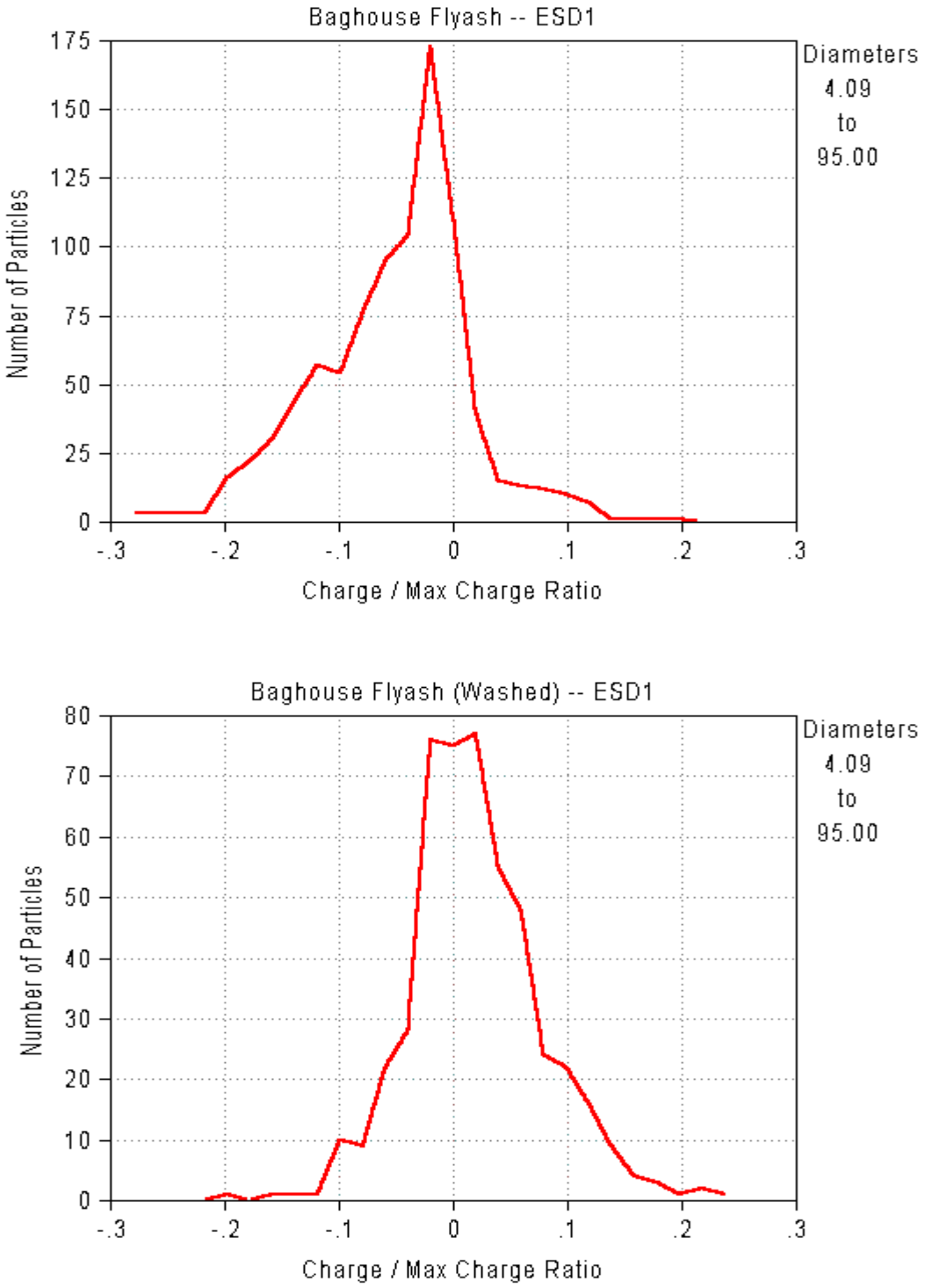

Figure 25. Charge distributions for flyash blown through a coiled copper tube. The top curve is for flyash as received. The bottom curve is after first dispersing the flyash in waster, filtering and drying it. A particle specific gravity of 1.5 was assumed for the calculation of charge.

Table C.I Charge summary for flyash as received and measured with the Particle Image Analyzer. (File: FASH01.PD)

	Dia	------- Negative -------			------- Positive -------			Total
No.	(um)	Count	fC	uC/g	Count	fC	uC/g	uC/g
1	4.09	31	-8.65	-9.53	2	0.10	1.70	-8.85
2	4.50	34	-10.34	-7.81	4	0.84	5.40	-6.42
3	4.95	40	-14.84	-7.16	5	0.95	3.65	-5.96
4	5.44	53	-24.30	-6.65	4	0.62	2.23	-6.02
5	5.99	55	-28.66	-5.67	7	1.07	1.66	-4.85
6	6.59	67	-37.12	-4.53	6	1.80	2.46	-3.96
7	7.25	44	-28.70	-4.01	5	1.87	2.30	-3.37
8	7.97	56	-43.59	-3.60	5	1.70	1.57	-3.17
9	8.77	45	-31.28	-2.41	2	1.37	2.38	-2.21
10	9.64	39	-28.74	-1.92	1	0.83	2.16	-1.82
11	10.61	36	-38.45	-2.09	4	4.01	1.96	-1.69
12	11.67	22	-25.49	-1.70	6	4.85	1.19	-1.08
13	12.84	20	-23.50	-1.30	6	5.87	1.08	-0.75
14	14.12	15	-23.10	-1.28	9	17.77	1.64	-0.18
15	15.53	13	-29.38	-1.41	4	9.32	1.45	-0.74
16	17.09	11	-29.48	-1.26	5	16.48	1.55	-0.38
17	18.80	8	-26.23	-1.16	2	3.15	0.55	-0.81
18	20.67	10	-30.47	-0.81	6	21.58	0.95	-0.15
19	22.74	8	-29.19	-0.73	2	12.29	1.22	-0.34
20	25.02	9	-57.62	-0.96	4	29.74	1.11	-0.32
21	27.52	14	-110.21	-0.88	6	42.73	0.80	-0.38
22	30.27	16	-97.98	-0.52	2	16.33	0.69	-0.38
23	33.30	4	-29.64	-0.47	0	0.00	0.00	-0.47
24	36.63	6	-47.82	-0.38	1	35.86	1.71	-0.08
25	40.29	9	-91.61	-0.36	1	48.21	1.72	-0.16
26	44.32	8	-93.34	-0.31	0	0.00	0.00	-0.31
27	48.75	7	-112.94	-0.33	1	7.06	0.14	-0.27
28	53.62	2	-17.08	-0.13	0	0.00	0.00	-0.13
29	58.99	1	-10.34	-0.12	1	62.01	0.71	0.29

	Negative	Positive	Neutral	Total
Count	683	101	111	895
Mass (nano-gram)	1962.33	373.01	305.07	2640.41
Charge (femto-C)	-1180.08	348.42		-831.67
Charge/Mass (uC/g)	-0.60	0.93		-0.36

Particle density = 1.50 g/cm^3
Max particle charge (neg) = -42.35 femto-C
Max particle charge (pos) = 62.01 femto-C
Count Median Diameter = 8.174 micrometers
Mass Median Diameter = 39.442 micrometers
Count Weighted Geometric Std. Deviation = 1.846
Mass Weighted Geometric Std. Deviation = 1.624

Table C.II. Charge Summary for flyash following water treatment. (File: FASH03.PD)

	Dia	------- Negative -------			------- Positive -------			Total
No.	(um)	Count	fC	uC/g	Count	fC	uC/g	uC/g
1	4.09	3	-0.50	-5.66	8	1.89	8.07	4.32
2	4.50	1	-0.06	-1.54	13	4.27	8.43	7.72
3	4.95	2	-0.22	-2.11	9	1.89	4.06	2.94
4	5.44	2	-0.53	-3.83	21	7.22	4.98	4.22
5	5.99	7	-1.49	-2.32	15	6.39	4.64	2.43
6	6.59	8	-2.58	-2.64	10	4.90	4.01	1.05
7	7.25	15	-3.90	-1.60	22	9.36	2.61	0.91
8	7.97	9	-2.64	-1.36	19	7.17	1.74	0.75
9	8.77	14	-5.94	-1.47	26	15.30	2.04	0.81
10	9.64	8	-5.53	-1.80	10	6.63	1.73	0.16
11	10.61	10	-6.02	-1.18	15	8.69	1.14	0.21
12	11.67	7	-8.50	-1.79	16	19.01	1.75	0.67
13	12.84	9	-9.30	-1.14	11	12.73	1.28	0.19
14	14.12	5	-4.74	-0.79	8	9.48	0.98	0.30
15	15.53	5	-10.03	-1.25	8	14.33	1.12	0.21
16	17.09	9	-11.27	-0.59	2	6.94	1.63	-0.18
17	18.80	7	-10.49	-0.53	5	7.34	0.52	-0.09
18	20.67	5	-15.24	-0.81	3	13.97	1.23	-0.04
19	22.74	6	-29.19	-0.97	5	21.51	0.86	-0.14
20	25.02	1	-1.86	-0.28	8	61.34	1.15	0.99
21	27.52	2	-15.74	-0.88	9	62.98	0.79	0.48
22	30.27	4	-46.27	-0.98	5	46.27	0.78	0.00
23	33.30	2	-6.59	-0.21	1	6.59	0.42	0.00
24	36.63	0	0.00	0.00	3	19.92	0.32	0.32
25	40.29	4	-33.75	-0.30	0	0.00	0.00	-0.30
26	44.32	0	0.00	0.00	5	81.67	0.44	0.44
27	48.75	2	-42.35	-0.43	3	91.77	0.62	0.20
28	53.62	2	-17.08	-0.13	0	0.00	0.00	-0.13

	Negative	Positive	Neutral	Total
Count	149	260	75	484
Mass (nano-gram)	579.88	736.59	284.26	1600.73
Charge (femto-C)	-291.79	549.55		257.76
Charge/Mass (uC/g)	-0.50	0.75		0.20

Particle density = 1.50 g/cm^3
Max particle charge (neg) = -28.24 femto-C
Max particle charge (pos) = 63.53 femto-C
Count Median Diameter = 10.077 micrometers
Mass Median Diameter = 39.206 micrometers
Count Weighted Geometric Std. Deviation = 1.802
Mass Weighted Geometric Std. Deviation = 1.614

Table C.III. Mass fraction and non-ash fractions for tribocharged and electrostatically separated flyash.

	Mass Fraction (%)		Non-Ash Fraction (%)	
	Run #1	Run#2	Run#1	Run#2
Positive Electrode	67.5	64.1	10.48	9.61
Negative Electrode	19.8	21.4	9.48	8.10
Filter	4.1	2.1	22.34	20.46

D. INSTRUMENT DEVELOPMENT

1. UV PHOTOELECTRON SPECTROSCOPE

Over the last few months I have continued work on an instrument to measure the work function of a sample through UV photoelectron spectroscopy in air. In Figure 26 a block diagram of the instrument is shown.

A complete description of how the instrument works is given in previous reports. The following is a brief overview; below the instrument a sample is illuminated with a tight frequency band of UV light. If the photons in this energy band are of sufficient energy electrons will be ejected from the surface. Since oxygen is electronegative, free electrons will most likely form negative O_2 ions. One ion is formed for each electron ejected from the surface. Hence, rather than finding the electron's kinetic energy, all of the electrons released can be counted by counting the ions. The electron yield is then plotted to extrapolate the cutoff frequency. This frequency correlates to the minimum photo energy required to eject an electron, which is the work function.

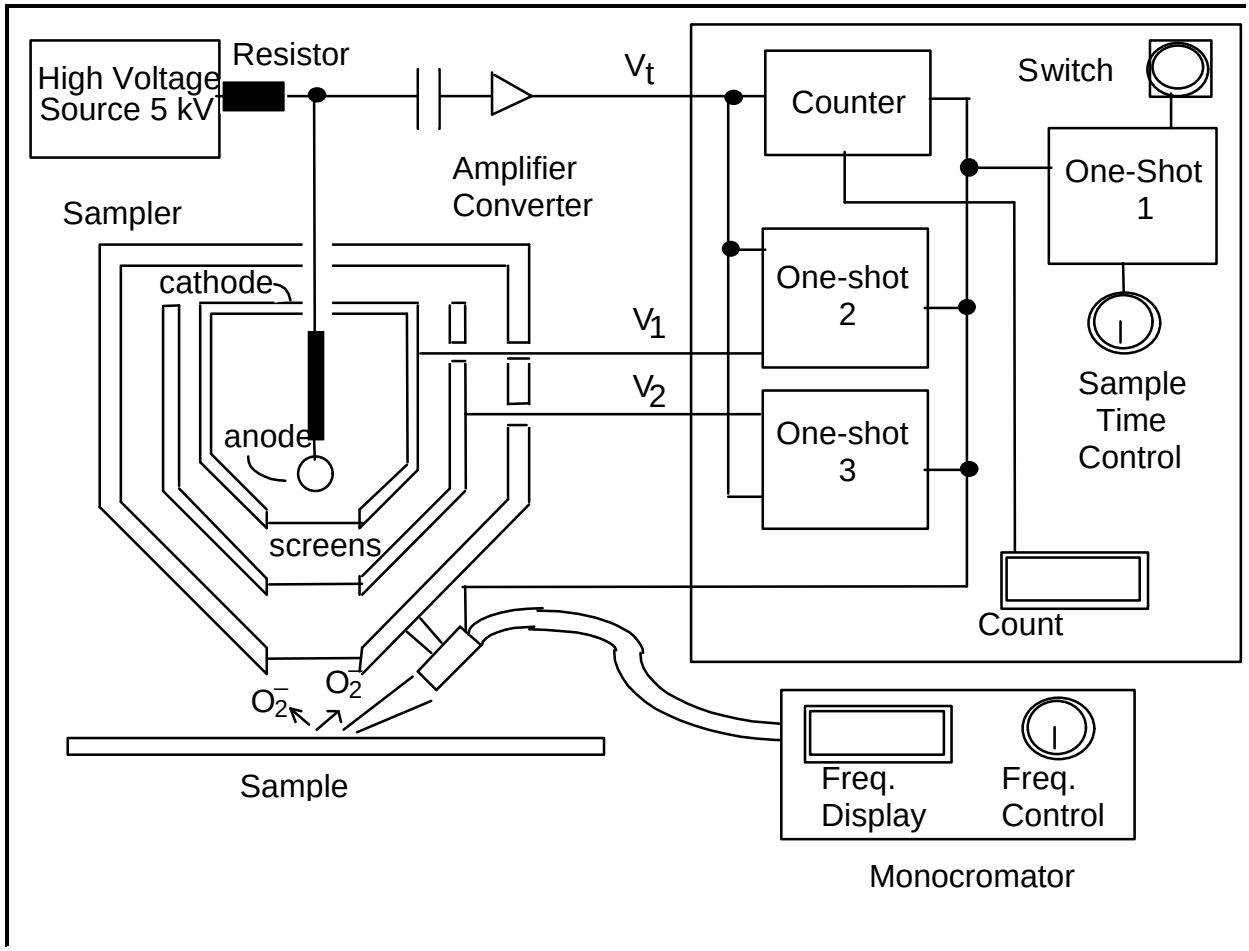

Figure 26. Block diagram of UV photoelectrom spectroscopy instrument.

Since the last report the mechanical components of the instrument have been completed. The anode shown in Figure 26 consists of a tungsten wire loop 6 mm in diameter. The loop was formed and then joined to an all-thread rod using silver solder and a flux consisting of potassium salts, fluorine and boron. The all thread rod was inserted into a threaded insulator at the top of the cathode chamber in Figure 26. The rod and screens can also be seen in the photograph of the instrument with its cover removed, Figure 29. This threaded rod allows the distance between the cathode and anode to be varied. Some initial tests have been preformed to determine the proper spacing between the cathode and anode. In these tests the spacing and the current between the cathode and anode were measured. The measured current was not what was expected, so some flaw in the anode may exist. Further tests on the nature of the discharge between the cathode and anode will need to be performed.

Also, since the last report, all of the controls for the instrument have been tested and mounted. Figures 27 and 28 show the components in the final instrument. In Figure 27 there is a small battery powered circuit that monitors for a voltage drop on the anode corresponding to a discharge between the anode and cathode. When the voltage drop is detected a light pulse from an LED is sent to a receiver in the control box on the top of the instrument. This allows the battery-powdered circuit to remain electrically isolated from the control circuits. Thus, the circuit can be floated at 5 kV. The control box was constructed and placed directly on top of the sensor unit to allow transmission of the light signal without the need for a fiber optic coupling.

Since the last report the electrical components of the instrument have been completed and tested as well. Both the battery-powered circuit and the control curcuit have been tested. Communication between the boards was tested using a 5mV 30kHz signal to simulate the maximum sample rate of the instrument as determined by its 3ms purging time. This also tested the counting rate of the output counter display. The total sample time generated by the control circuit was also tested and set at 8 s. Finally the circuits controlling the voltages to the suppression and quenching screens where completed and tested.

With the optical components finished by the last report and the mechanical and electrical components finished and tested the instrument is near completion. The correct spacing between the anode and cathode must still be determined. Also a problem isolating the battery-powered board from the outer-grounded housing must still be solved. Parts of the outer housing are being remade out of Lexan to prevent discharge from the battery-powered board to ground. Finally, some initial test samples must be selected to compare the result from the instrument to previously accepted values from the literature.

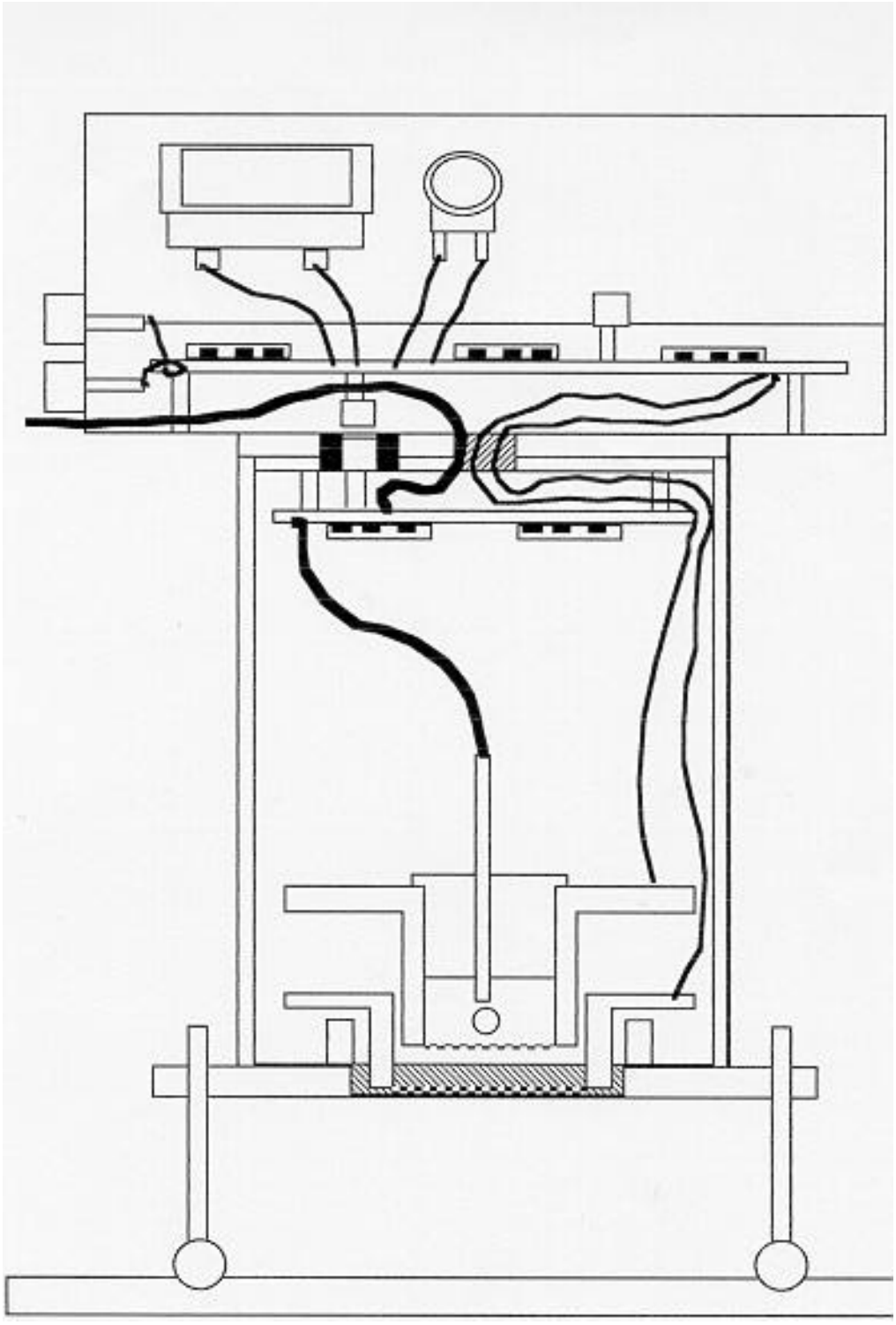

Figure 27. Cross sectional diagram of the UV photoelectron ion detector.

Figure 28. Photograph of the sensor head and control box of the UV photoelectron ion detector.

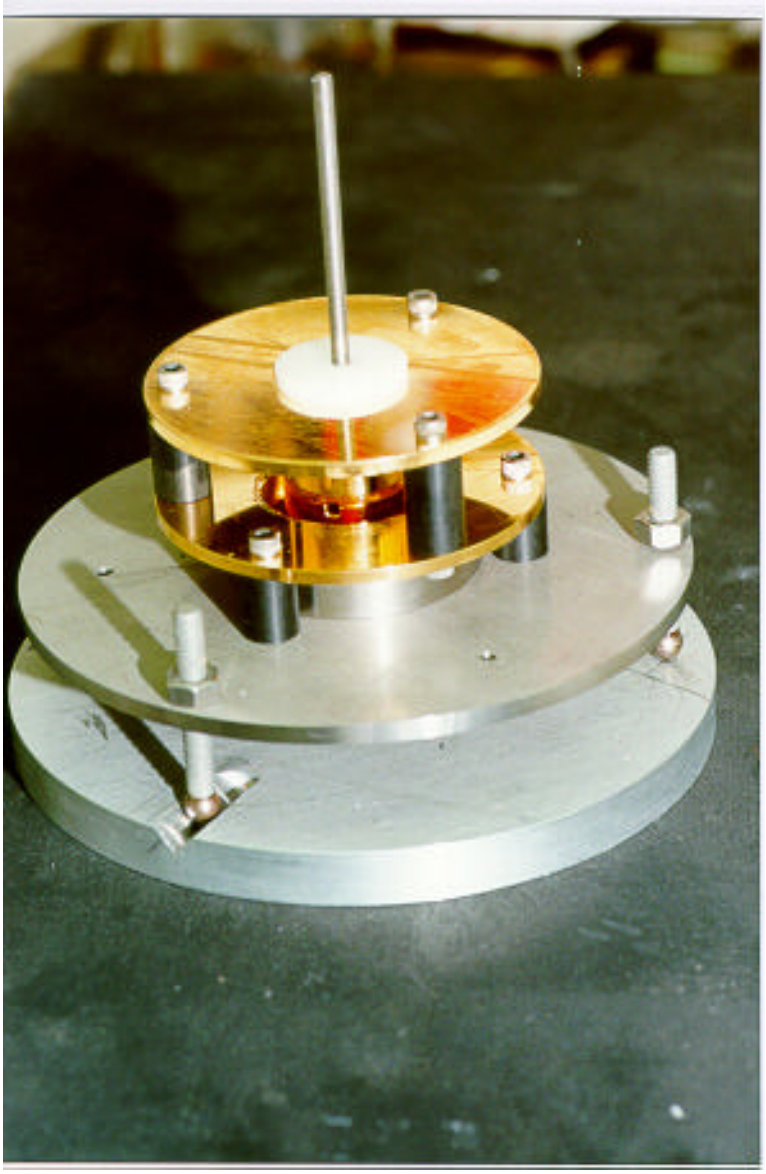

Figure 29. Photograph of the internal components of the sensor head showing screens and anode and cathode assemblies on the grounded base.

2. PARTICLE IMAGE ANALYZER

The video particle image analyzer was developed to measure size and charge of airborne particles. The last technical progress report discussed planned modifications. A dual Pentium II – 300 MHz computer system and a full frame progressive scan camera and frame grabber have been purchased. The high voltage transformer has been suitably modified and an audio amplifier has been purchased to drive it. We have constructed the measurement chamber and the lower section of the flow stabilization system.

Testing of the camera revealed a dead time of 2 to 3 milliseconds between the end of the integration for one frame and the beginning of integration for the next. This dead time would make the adjacent frame analysis scheme discussed in the last report less advantageous. We are looking at dual sensor cameras designed for particle image velocimetry, but for now we will use the algorithms used with the first PIA prototype. The inlet flow system modifications and considerations discussed in the last report have not yet been addressed.

Figures 30 through 32 show photos of the current state of the instrument. Figure 32 shows simulated traces on the computer screen. These along with traces from the first prototype store VCR tape are being used in the software development until we complete the electric drive and synchronization circuitry.

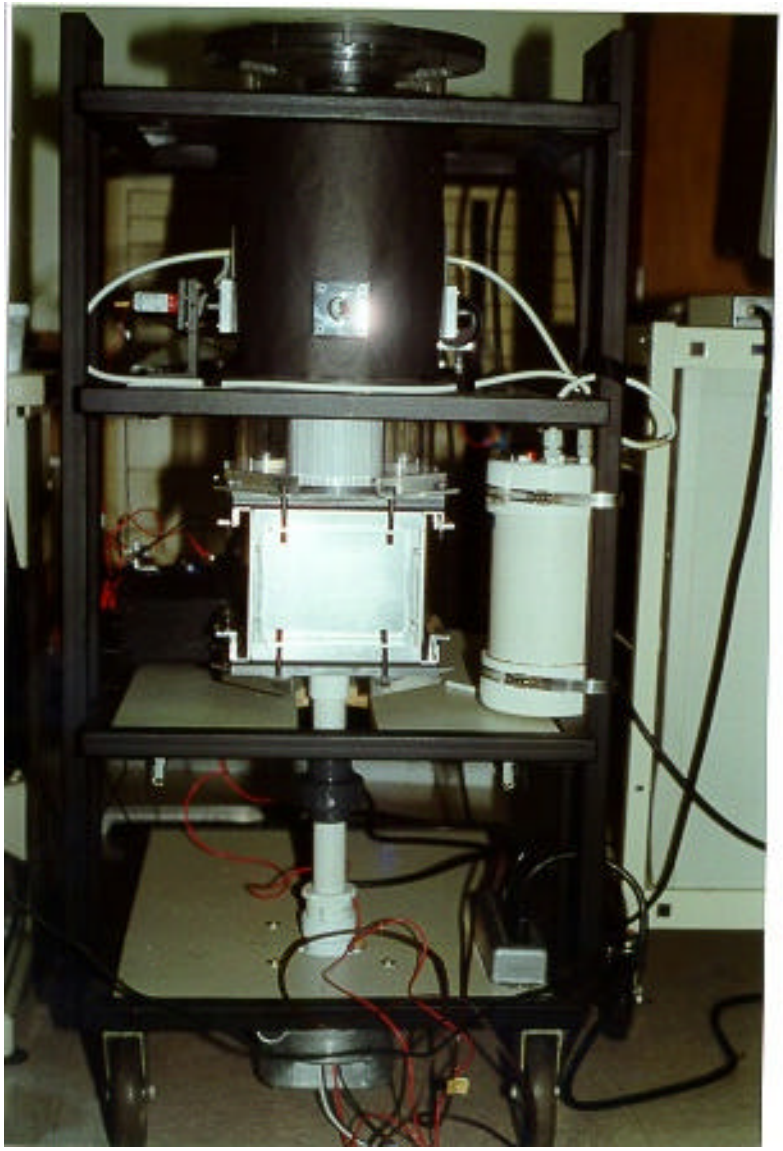

Figure 30. Photograph of current state of the particle image analyzer. The top section is the measurement chamber. The outer tube is covered with black paper. Collection optics are on the opposite side of the chamber. A diode laser line generator can be seen on the left side. The HEPA filter and high voltage transformer are visible in the center section. The blower fan is located under the bottom panel.

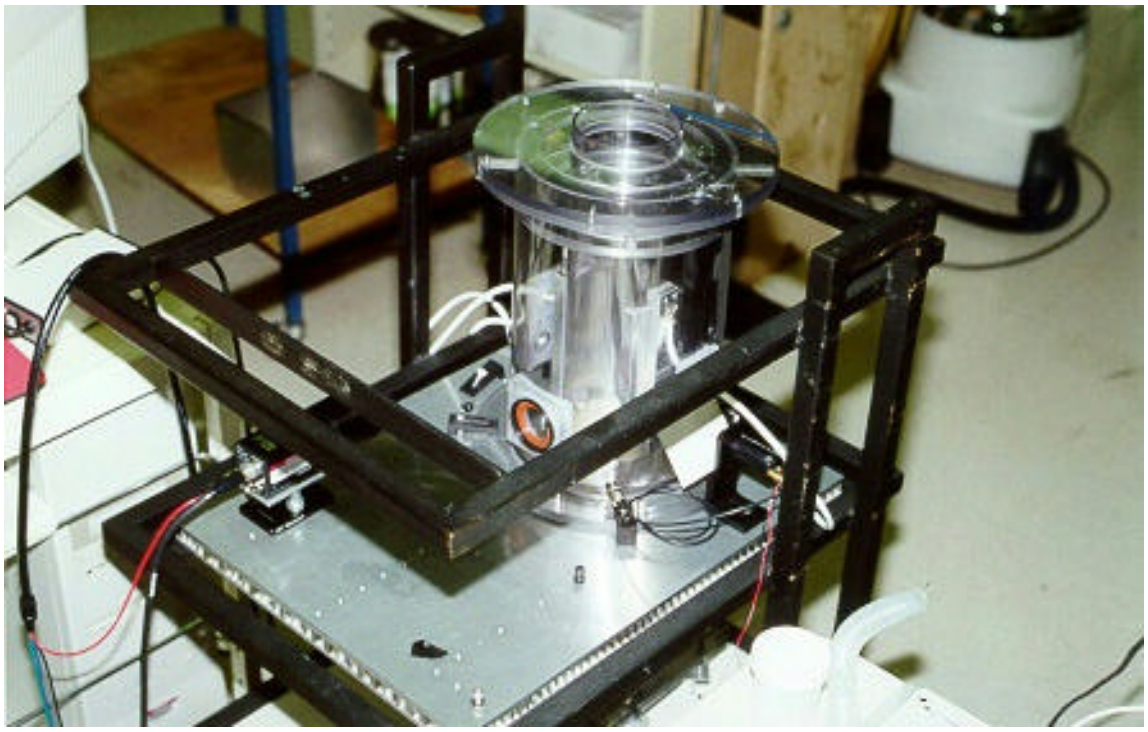

Figure 31. Measurement chamber of the particle image analyzer. The electrodes curve to the same radius (5cm) as the inner tube and are protected by an outer 10 cm radius outer Lexan tube. The receiving lens is not installed in this photo.

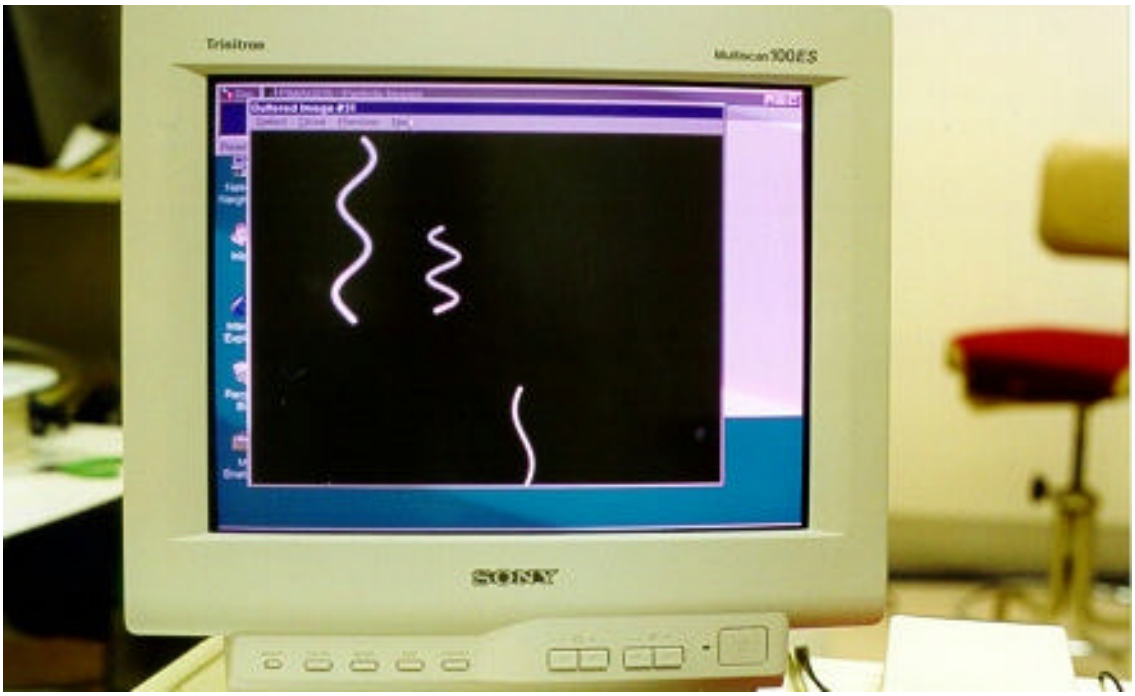

Figure 32. Simulated particle traces used during the software development.

3. CALIBRATION DROPLET GENERATOR

During this semester we began the development of a droplet generator for use in calibration of the Particle Image Analyzer and other airborne particle analyzers, such as the E-SPART, used in our department. We purchased the head of a continuous inkjet printer which we are modifying for our specific needs. The goal is to have a quick, simple method of generating monodisperse droplets of known size and charge. The continous ink jet system uses a piezoelectric transducer to periodically disrupt a liquid stream exiting a small orifice. Constant pressure produces a steady liquid flow while within a range of frequencies one droplet is produced for each vibration cycle of the transducer. Thus the droplet diameter remains fixed and can be calculated providing the liquid flow rate is known. The droplets are charged by induction by applying a voltage to an electrode near the orifice. The liquid usually consists of a volatile and a non-volatile component. The final droplet size can be controlled by varying the concentration of the non-volatile component.

Figure 33 shows a photograph of the printer head. Figure 34 shows images of the monodisperse droplets on a video monitor. An LED located behind the droplet jet is synchronously strobed while the droplets are observed with a video camera.

III. PLANS FOR THE CURRENT SEMESTER

In the coming semester the three instruments, UV photoelectron spectrometer (UPS), Particle Image Analyzer (PIA), and Calibration Droplet Generator will be completed. We will use the PIA to improve our analysis of tribocharging parameters. On completion of the PIA we will use it to determine charge-to-mass ratio distributions as a function of particle size distribution.

The UPS will be tested on insulating surfaces and then on polished coal surfaces and possibly on single particles. The UPS instrument together with a recent upgrade to our epi-fluorescent microscope will allow us to associate charge characteristics and work functions with different maceral and mineral types.

Further investigations will be made of two stage beneficiation.

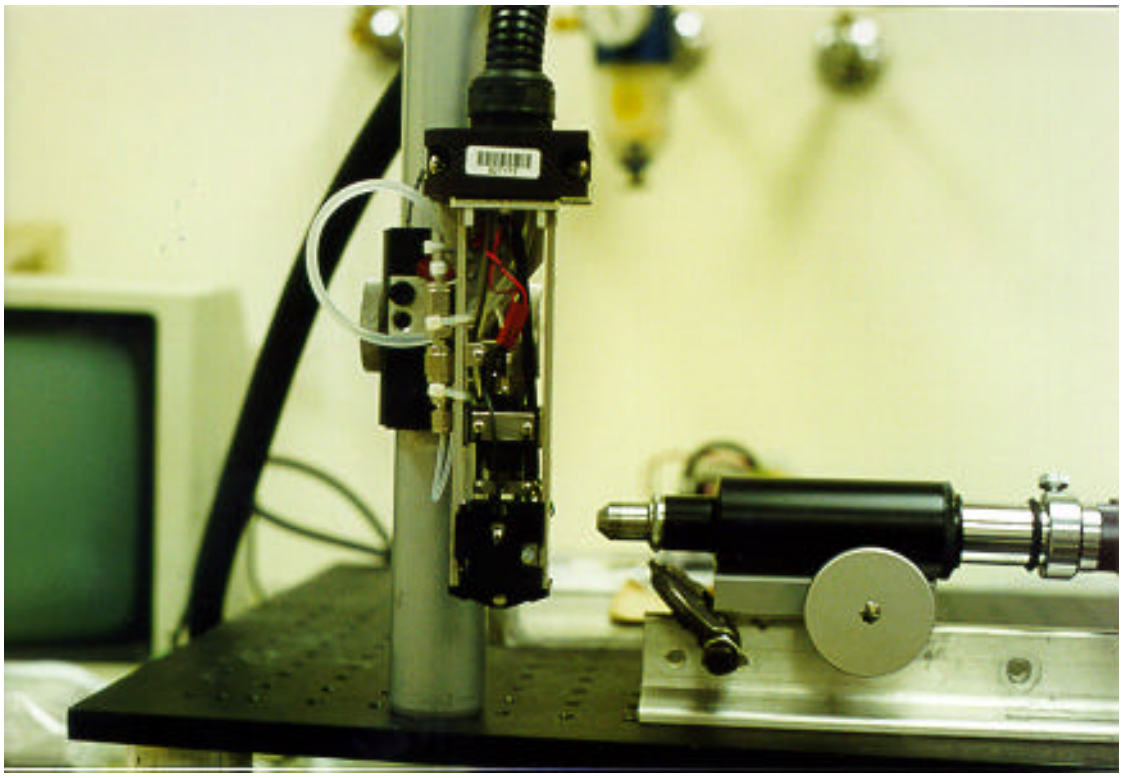

Figure 33. Ink jet printer head set up for viewing droplets with a video camera. The printer head is being modified for use as a calibration droplet generator.

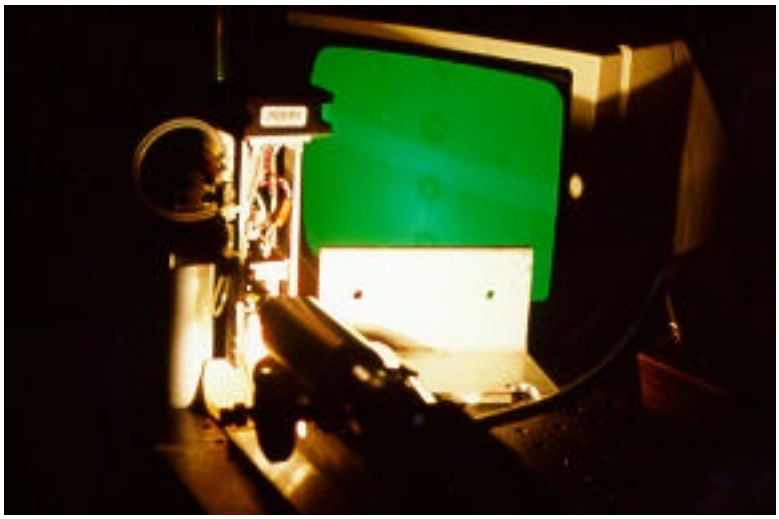

Figure 34. Photograph of the calibration droplet generator with a screen image of the monodisperse droplets in the background. The droplets are approximately 55 μm in diameter. The droplets are illuminated by a strobed LED, so that each droplet image on the video monitor screen represents light scattered from about 1000 droplets of the same size and in the same location at the time of the strobe.